



**Keywords:**

nuclear structure, electromagnetic transitions, ab initio theory, precision experiment

**Author for correspondence:**

R. Roth

e-mail:

[robert.roth@physik.tu-darmstadt.de](mailto:robert.roth@physik.tu-darmstadt.de)

# Electromagnetic properties of nuclei from first principles: a case for synergies between experiment and theory

R. Roth<sup>1,2</sup>, M. Petri<sup>3</sup>

<sup>1</sup> Institut für Kernphysik, Technische Universität Darmstadt, 64289 Darmstadt, Germany

<sup>2</sup> Helmholtz Forschungsakademie Hessen für FAIR (HFHF), 64291 Darmstadt, Germany

<sup>3</sup> School of Physics, Engineering and Technology, University of York, YO10 5DD York, UK

One of the overarching goals in nuclear science is to understand how the nuclear chart emerges from the underlying fundamental interactions. The description of the structure of nuclei from first principles, utilizing ab initio methods for the solution of the many-nucleon problem with inputs from chiral effective field theory, has advanced dramatically over the past two decades. We present an overview over the available ab initio tools with a specific emphasis on electromagnetic observables, such as multipole moments and transition strengths. These observables still pose a challenge for ab initio theory and are one of the most exciting domains to exploit synergies with modern experiments. Precise experimental data is vital for the validation of the theory predictions and the refinement of ab initio methods. We discuss some of the past and future experimental efforts highlighting these synergies.

## 1. Introduction

Atomic nuclei are finite quantum systems consisting of protons and neutrons. Their structure, i.e., how protons and neutrons arrange themselves and how they interact among each other to form complex nuclei, has a decisive impact on everyday life, from the very existence of carbon-based life on earth to critical nuclear physics applications such as carbon dating. Describing the nuclear structure from first principles, i.e., from fundamental interactions between its constituents based on the theory of the strong interaction, quantum chromodynamics (QCD), is hence pivotal in our understanding of the physical world and has been a focus of nuclear science for many decades. Despite the fact that nuclei and their structure have been the subject of vigorous studies for more than a century, their understanding is still mostly based on phenomenological considerations. The understanding of nuclei from first principles (rooted in QCD) will offer strong predictive power with direct implications to other science frontiers, such as neutrino physics (tackling the nuclear matrix element uncertainties) and astrophysics (determining astrophysical reaction rates and understanding the origin of the elements).

A theoretical concept that brings nuclear structure physics closer to reaching this goal exploits chiral effective field theories (EFTs) of the strong interaction, as first proposed by Steven Weinberg [1], to derive nuclear interactions [2–4]. These interactions are the foundation of modern *ab initio* methods, such as Nuclear Lattice EFT, the No-Core Shell Model (NCSM), and different medium-mass methods, like the Coupled Cluster approach or In-Medium Similarity Renormalization Group. Built on the same foundation, these methods allow for a complementary access to nuclear structure observables, as illustrated in Figure 1, allowing for a validation of the methods by direct comparison of observables. Moreover, a broad range of systems can be targeted with the various methods, ranging from stable and neutron-rich nuclei to the equation of state for neutron-star matter [5]. The three-nucleon (3N) forces play a prominent role in neutron-rich nuclear systems [6] and they emerge naturally in EFT allowing for a systematic study of their effect in the evolution of nuclear structure towards the limits of nuclear existence.

Key to further advancing the frontiers of *ab initio* theory are pioneering experiments on atomic nuclei that confront *ab initio* predictions and provide unparalleled benchmarks for the development and refinement of the theoretical approaches. In this contribution, we highlight some of the developments at the *ab initio* frontier and we put forward selected experimental efforts (both past and future) that aim at validating these calculations, with a particular focus on experimental work that has been fostered from robust synergies of experiment and theory. We focus on electromagnetic observables, which present a particular challenge for *ab initio* theory, as will be discussed in the following.

## 2. *Ab initio* theory towards electromagnetic observables

### (a) Background—The early days

The *ab initio* description of nuclear structure in a modern sense started more than two decades ago with the first calculations using realistic nucleon-nucleon (NN) and three-nucleon (3N) interactions. While initial calculations were limited to few-body systems [7], two different *ab initio* many-body methods paved the way towards heavier systems: The Green's Function Monte-Carlo (GFMC) approach [8,9] and the No-Core Shell Model (NCSM) [10,11]. With these methods the focus expanded from ground-state observables and continuum processes, which are the main targets in few-body studies, to spectroscopy, i.e., the description of excitation spectra and electromagnetic moments and transitions.

These methods encounter the need to introduce controlled approximations and truncations. While in few-body calculations the consensus is that all technical discretizations and truncations hidden in the numerical treatment are sufficiently converged to consider the results to be quasi-exact, the GFMC and NCSM always have to fight for convergence. In GFMC the noise associated

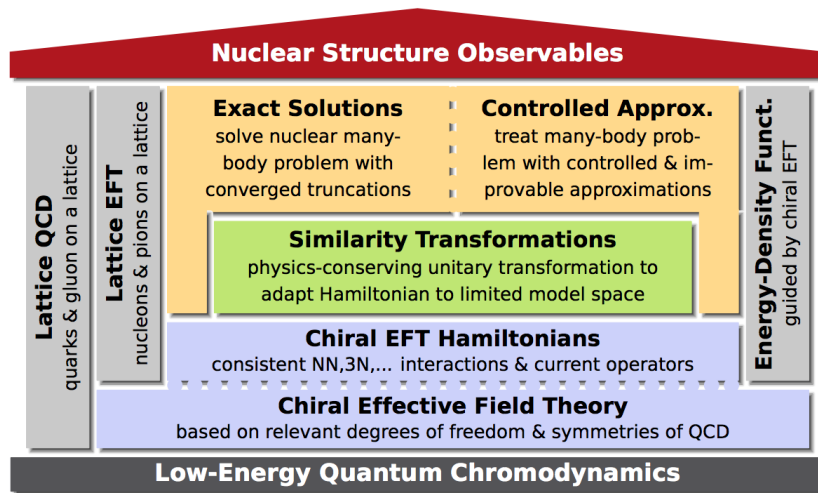


**Figure 1.** Connecting nuclear structure with low-energy QCD. The direct route is through lattice QCD calculations, however, these calculations are computationally demanding, are currently limited to few-nucleon systems and their accuracy is insufficient for precision nuclear physics. Chiral Effective Field Theory of the strong interaction allows us to derive nuclear interactions and Hamiltonians that can be used in a suite of different many-body methods and link nuclear structure observables with low-energy QCD.

with Monte-Carlo sampling and the convergence of the observables in the imaginary time propagation limit the final precision. For the NCSM the truncation to a finite model space and the convergence of observables with increasing model-space dimension set the limits.

In both cases, the convergence limitations rapidly get worse with increasing particle number and effectively restrict the range of nuclei that can be addressed. Even today, the limit for the original formulations of GFMC and NCSM are in the regime of p-shell nuclei, with  $^{12}\text{C}$  being among heaviest nuclei that has been studied in detail [9,12].

A first cornerstone of modern advances of ab initio nuclear structure theory is, therefore, the development of new and improved many-body methods to extend the ab initio domain to heavier nuclei. Some of these new methods build on the basic ideas of the first-generation ab initio methods, i.e., GFMC and NCSM, and tackle the convergence limitations in different ways. We will discuss examples for NCSM-based methods in section 2(b). Other methods attack the many-body Schrödinger equation from a different angle, leading to the so-called medium-mass approaches. We will go into more detail on these second-generation ab initio methods in section 2(c).

Besides the advances on the formal approach to the nuclear many-body problem, a second cornerstone is the rapid developments in algorithms and computing power. From the beginning, ab initio calculations were limited by computational capabilities and capacities. Improvements in algorithms and implementations, the use of massively parallel computing architectures and graphics processing units, and the general growth of computing power available with modern supercomputers all translate into an extension of the reach of ab initio methods.

A third cornerstone for modern ab initio theory is chiral effective field theory (EFT). All ab initio solutions of the many-body problem need a well-defined Hamiltonian as a starting point. Since we are working with nucleons as effective degrees of freedom in our many-body approach, the Hamiltonian and the inter-nucleon interactions contained in it represent the link to the underlying theory of the strong interaction. As such, the nucleonic interactions encapsulate all the complexity of the quark-gluon-physics of quantum chromodynamics (QCD).

It is a formidable task to construct the nucleonic interactions based on the dynamics. The first-generation ab initio calculations used phenomenological interactions, such as the Argonne or Bonn family of interactions [13,14], which accurately reproduced two-nucleon scattering phase shifts but were rather ad hoc in their construction. Practically all of today's ab initio calculation use interactions from chiral EFT as starting point and typically two-nucleon (NN) and three-nucleon (3N) interaction are being included [2–4]. Chiral EFT offers two decisive advantages over phenomenological approaches: systematicity and consistency. Just like the many-body approaches, chiral EFT employs a truncation to render an infinite expansion finite. The expansion and truncation is implemented via a power counting in a small expansion parameter connected to the momentum scale of the system. With increasing order of the chiral truncation we expect a convergence of the interactions implying a convergence of observables computed with these interactions. Therefore, chiral EFT offers a systematic way to improve the description by going to higher orders of the expansion—this is what we refer to as systematicity. Consistency refers to the possibility to extract interactions of different particle rank (NN, 3N, and beyond) as well as electromagnetic and weak operators in a coherent and consistent framework. We are only starting to exploit these features of chiral EFT today.

The fourth and final cornerstone of today's ab initio theory is uncertainty quantification. For a long time, many theoretical results and predictions in nuclear structure theory were presented as raw numbers for a given nuclear observable without any qualification of their reliability. In some cases, these numbers are supplemented by statements about expected error bars, based on vague general arguments and expectations (expert assessment). In some cases, a more systematic uncertainty quantification is applied for one specific source of uncertainty, e.g., the model-space truncation of the many-body approach. However, the preceding discussion shows that an observable extracted from an ab initio calculation is subject to a number of different choices and truncations. Already the many-body methods themselves employ one or more truncations plus varying approximations. A classical NCSM calculation is probably the simplest example, being built on just a single many-body truncation and no additional approximations. For the medium-mass methods several truncation and approximations are involved. Also the formulation of the chiral EFT interactions utilizes truncations, mainly the chiral order, and choices, such as the regular scheme and scale, and experimental uncertainties through the fit to data in few- and many-body systems. All of these uncertainties are correlated and a comprehensive uncertainty quantification is challenging and subject of present research [15–17].

## (b) No-core shell model

As a baseline for a more detailed discussion and a first glimpse at the special difficulties we encounter with electromagnetic observables, we will present the NCSM in a little more detail.

**Hamiltonian.** We start with a Hamiltonian  $H$  which includes the kinetic energy  $T$  of the nucleons and the chiral interactions mentioned earlier, for simplicity we restrict ourselves to NN and 3N interactions,  $V_{\text{NN}}$  and  $V_{\text{3N}}$ . A detail already relevant at this stage is translational invariance—all intrinsic nuclear properties should be independent of the center-of-mass motion of the nucleus. In the ideal case the many-body state resulting from the ab initio solution should factorize into a product of an intrinsic and a center-of-mass state. This can be achieved in a classical NCSM calculation using the harmonic-oscillator basis, however, general basis sets or other many-body truncations destroy this exact factorization. A minimal requirement for all ab initio calculations is that the operator representing the observables are formulated in a translationally invariant manner. This is relevant for all the observables that appear in the calculation. For the Hamiltonian it implies that we have to use the intrinsic kinetic energy  $T_{\text{int}} = T - T_{\text{cm}}$  which results from the subtraction of the kinetic energy of the center-of-mass motion  $T_{\text{cm}}$  from the total kinetic energy. The generic Hamiltonian thus reads

$$H = T_{\text{int}} + V_{\text{NN}} + V_{\text{3N}}, \quad (2.1)$$

where the Coulomb interaction among protons is absorbed in the NN interaction operator.

**Many-Body Schrödinger Equation.** For this Hamiltonian, we aim to solve the eigenvalue problem in an  $A$ -nucleon Hilbert space, i.e., the many-body Schrödinger equation

$$H |\Psi_n\rangle = E_n |\Psi_n\rangle \quad (2.2)$$

with nuclear eigenstates  $|\Psi_n\rangle$  and the corresponding energy eigenvalues  $E_n$ . All ab initio methods are tackling this equation in some form, often by reformulating the eigenvalue problem in a computationally more convenient form. The NCSM attacks the eigenvalue problem directly as such, using a computationally accessible basis representation. In its standard formulation the NCSM uses  $A$ -body Slater determinants  $|\Phi_\nu\rangle$  of discrete single-particle harmonic oscillator (HO) states for a specific oscillator frequency  $\hbar\Omega$ . This infinite basis is truncated with respect to the total HO excitation energy  $N_{\max}\hbar\Omega$  of the basis determinants above the energetically lowest  $A$ -body Slater determinant. For any finite value of  $N_{\max}$  the basis determinants span a finite model space  $\mathcal{M}(N_{\max})$  and thus lead to a finite matrix eigenvalue problem

$$\sum_{\nu' \in \mathcal{M}(N_{\max})} \langle \Phi_\nu | H | \Phi_{\nu'} \rangle C_{\nu'}^n(N_{\max}) = E_n(N_{\max}) C_\nu^n(N_{\max}) \quad \text{for all } \nu \in \mathcal{M}(N_{\max}). \quad (2.3)$$

The numerical solution of this matrix eigenvalue problem for fixed  $N_{\max}$  yields energy eigenvalues  $E_n(N_{\max})$  and, via the eigenvectors, the expansion coefficients for the eigenstates

$$|\Psi_n(N_{\max})\rangle = \sum_{\nu \in \mathcal{M}(N_{\max})} C_\nu^n(N_{\max}) |\Phi_\nu\rangle. \quad (2.4)$$

Note that we explicitly indicated the dependence of the energy eigenvalues and the eigenstates on the truncation parameter  $N_{\max}$ .

**Convergence.** In the limit  $N_{\max} \rightarrow \infty$ , i.e., the model space approaches the full Hilbert space, these quantities are guaranteed to coincide with the formally exact solutions of the many-body Schrödinger equation (2.2), i.e.,

$$E_n(N_{\max}) \rightarrow E_n \quad \text{and} \quad |\Psi_n(N_{\max})\rangle \rightarrow |\Psi_n\rangle \quad \text{for } N_{\max} \rightarrow \infty. \quad (2.5)$$

The approach to this limit is what we call the model-space convergence. It is a great advantage of the NCSM that there is a single control parameter,  $N_{\max}$ , which governs the precision and allows for a systematic improvement of the calculation. For the energy eigenvalues, the NCSM at any  $N_{\max}$  constitutes a variational approximation and the convergence of the eigenvalue with increasing  $N_{\max}$  proceeds monotonically from above. This provides an additional level of control and facilitates extrapolation schemes that aim to improve the results beyond the precision reached at the largest attainable  $N_{\max}$  truncation.

While we obtain ground- and excited-state energies directly from the eigenvalues, other observables like radii, electromagnetic moments, or transition strengths have to be computed as expectation values or off-diagonal matrix elements from the eigenvectors  $|\Psi_n(N_{\max})\rangle$ . They will also exhibit an observable-specific convergence pattern, which often is very different from and more complicated than the energy.

The crucial question in all practical application is: Can we reach sufficiently converged observables within the computational limits for  $N_{\max}$ ? Due to the low-energy or low-momentum character of the Hamiltonian, which is built with interactions that use an explicit momentum cutoff, we expect that observables will converge to their exact value well before the formal limit  $N_{\max} \rightarrow \infty$ . However, due to the factorial growth of the model-space dimension and, thus, the size of the matrix eigenvalue problem, we will be computationally limited to a rather limited range of  $N_{\max}$ ; for a mid-p-shell nucleus  $N_{\max} = 10$  is typically the maximum that can be reached even with supercomputer resources. For heavier nuclei this computational limit drops even lower and hampers the applicability of the NCSM. Even with soft cutoff-regularized chiral interactions, it is not possible to reach a sufficiently converged result within these limits. Therefore, several

additional measures are being used to improve the scheme. They can be grouped in three categories: pre-processing, optimization, and post-processing.

**Pre-Processing.** One option to improve on the convergence limitations of the NCSM and of many other ab initio method is a pre-processing of the Hamiltonian. Already the first ab initio applications of the NCSM used a similarity transformation in the form of the Okubo-Lee-Suzuki approach [11,18] to implement a decoupling of the model space to accelerate the convergence. A more flexible and universal approach and the present default for implementing a generic pre-diagonalization of the Hamiltonian is the similarity renormalization group (SRG) [19–22]. The SRG is built on a unitary transformation with a continuous parameter, the flow parameter, which is implemented via a Heisenberg-like differential equation, the flow equation,

$$\frac{dH(\alpha)}{d\alpha} = [\eta(\alpha), H(\alpha)]. \quad (2.6)$$

The flow equation defines an initial value problem, with the initial Hamiltonian  $H(\alpha=0)$  given by (2.1). The change of the Hamiltonian throughout the flow evolution is governed by the generator  $\eta(\alpha)$  which can be designed to achieve specific decoupling patterns. The standard choice for the pre-processing is

$$\eta(\alpha) \propto [T_{\text{int}}, H(\alpha)], \quad (2.7)$$

which effects a pre-diagonalization of the Hamiltonian in momentum space [21,22]. Note that all these expressions are operator equations, just like the initial many-body Schrödinger equation (2.2). In order to solve them numerically, we again use a truncated basis representation. In addition we use a cluster decomposition, i.e., we decompose the evolved Hamiltonian into irreducible one-, two-, three- and many-body contributions and compute the individual contributions separately. This cluster expansion has to be truncated as well, since beyond the three-body contribution the solution of the flow equation in sufficiently large basis sets becomes prohibitive.

The unitarity of the transformation guarantees that the eigenvalues of the transformed Hamiltonian are the same as for the initial operator. Likewise the expectation values of other observables computed with the eigenstates of the transformed Hamiltonian remain invariant if the observable is transformed consistently with the Hamiltonian. The correlations that are removed from the eigenstates through the pre-diagonalization show up as additional contributions to the operators of the observables. This unitary invariance of eigenvalues and expectation values holds as long as the SRG transformation does not involve additional truncations. The restriction of the transformed operators to two- or three-body rank, however, formally breaks unitarity at the  $A$ -body level and induces uncertainties.

**Optimization.** We can also improve the NCSM calculation itself to reach better convergence without increasing the computational cost. We can, for example, consider a different single-particle basis than the HO. The HO oscillator basis has unique properties from the formal point of view, in that it allows for the exact factorization of the center of mass and, related to that, an analytic transition from single-particle to relative coordinates through the Talmi-Moshinsky transformation. These tools are extensively used in the computation of matrix elements, therefore, the first steps in an NCSM-type calculation will benefit from using the HO basis. However, the HO wave functions, particularly regarding their long-range Gaussian fall-off, are not optimal for the description on a self-bound nuclear system, where we expect an exponential asymptotic for the wave function. We could imagine an optimized single-particle basis, which takes the correct asymptotic behavior and gross properties of the many-body system, e.g., its size, into account in a nucleus and interaction-specific way. The so-called natural-orbital basis [23] provides these benefits and was shown to yield an optimal convergence rate for energies.

Another way to optimize an NCSM calculation is to further reduce the basis dimension within a given  $\mathcal{M}(N_{\text{max}})$  model space. When we analyze the contribution of individual basis states to

low-lying eigenstates of the Hamiltonian for a specific nucleus, we find that many basis states exhibit very small or vanishing coefficients in (2.4). Omitting these basis states from the beginning would not change the eigenstates significantly, but reduce the dimension of the matrix eigenvalue problem to be solved. We can estimate the expected coefficients of individual basis states using perturbation theory, which leads to a state-selective a priori importance measure. By introducing a truncation threshold on this importance measure we can define an importance-truncated model space, which is significantly smaller than the full  $\mathcal{M}(N_{\max})$ . Eventually this importance truncated NCSM [24,25] enables us to go beyond the  $N_{\max}$  limits of the standard NCSM.

**Post-Processing.** In order to assess the convergence behavior of an NCSM calculation we always perform multiple eigenvalue solutions for a range of  $N_{\max}$  truncation parameters. Thus we will obtain a sequence of values for any of the observables within a certain range of  $N_{\max}$ . In many cases, we will not reach complete convergence within these sequences, but we can use them to predict or extrapolate a converged value of an observable. Particularly for energies, with their monotonic convergence pattern, heuristic extrapolation schemes based on, e.g., exponential parametrizations have been used routinely [26]. Attempts have been made to explain the behavior of converging sequences within an effective theory to obtain physics-based model for the dependence of an observable on the model-space parameters [27–30]. Still, the extrapolations of observables other than the energies are difficult because of their more complex and varied convergence patterns.

A recent development is the use of machine learning and artificial neural networks for the prediction of converged observables [31–33]. In these data-driven approaches large sets of actual NCSM calculations are being used to train an artificial neural network to predict the converged values of the observable. Unlike the extrapolation schemes, which rely on a physically motivated parametrization of the model-space dependence of the observable, the neural networks learn this behavior from the actual calculations. We have designed a universal class of neural networks which uses NCSM data from light nuclei, where the exact, i.e., fully converged results are accessible, for the training process. We have shown that the trained networks can then be applied for arbitrary nuclei and provide robust predictions with statistically meaningful uncertainties [33]. For the first time, this scheme allows for robust and accurate predictions for nuclear radii also in cases with difficult convergence patterns [34].

### (c) Medium-mass methods

Despite all the improvements, the range of nuclei accessible to the NCSM is limited to the  $p$  or lower  $sd$ -shell and the fundamental reason for this limitation is the factorial growth of the problem dimension with particle number. Such a drastic scaling is the curse of all approaches that build on a direct basis expansion, including the so-called full configuration interaction (CI) approaches that use a truncation of the underlying single-particle basis. In order to counteract this curse of dimensionality, one can employ a more drastic basis truncation on the number of particle-hole excitations on top of a reference state. The reference state  $|\Phi_{\text{ref}}\rangle$  can be thought of a rough approximation of the ground state of the nucleus and, in many cases, might be limited to a single Slater determinant suitable for the description of closed-shell systems. We can define particle-hole excitations on top of  $|\Phi_{\text{ref}}\rangle$  and in this way organize the complete many-body basis of a full CI calculation. With second quantization creation and annihilation operators, we can write the particle-hole expansion of a CI eigenstate as

$$\begin{aligned} |\Psi_{\text{CI}}\rangle &= C |\Phi_{\text{ref}}\rangle = (C_0 + C_1 + C_2 + \dots) |\Phi_{\text{ref}}\rangle \\ &= \left( C_0 + \sum_{ph} C_{ph} a_p^\dagger a_h + \sum_{pp'hh'} C_{pp'hh'} a_p^\dagger a_{p'}^\dagger a_{h'} a_h + \dots \right) |\Phi_{\text{ref}}\rangle \end{aligned} \quad (2.8)$$

with coefficients sets  $C_0, C_{ph}, C_{pp'hh'}, \dots$  determined from the eigenvalue solution. This basis organization enables an additional truncation with respect to the particle-hole rank, e.g., by

omitting all terms beyond the two-particle-two-hole (2p2h) level. This will drastically reduce the basis dimension and tame the scaling, but will also significantly limit the ability of the basis to capture many-body correlations, particularly collective correlations build from multi-particle-multi-hole excitations.

Therefore, a central theme for the many-body methods discussed in the following is to enhance the ability to capture the many-body correlations as compared to a simple particle-hole truncated basis expansion without increasing the problem dimension. As a result, the numerical character of the problem changes—from a matrix eigenvalue problem to coupled sets of nonlinear equations or differential equations. This is where we enter the realm of the so-called medium-mass methods.

In the following we discuss the basic conceptual ideas for a selection of medium-mass methods. This selection cannot be exhaustive, and we will not address propagator-based and perturbative methods, such as self-consistent Green's function methods [35], quantum Monte Carlo methods [36–38], or advanced implementations of many-body perturbation theory [39]. We also do not cover symmetry-driven methods, such as the symmetry-adapted NCSM [40], and methods based on symmetry breaking and restoration, e.g., generator coordinate methods combined with the in-medium SRG [41] or multi-reference many-body perturbation theory [42,43]. However, it should be noted that these methods hold great potential for the description of electromagnetic properties for heavier nuclei.

**Coupled-Cluster Theory.** Coupled cluster theory nicely illustrates the step away from a linear basis expansion of the eigenstates (2.8) to a more powerful ansatz for the many-body ground-state. Starting from a single-determinant reference state  $|\Phi_{\text{ref}}\rangle$ , correlations are added through the application of an exponential wave operator

$$|\Psi_{\text{CC}}\rangle = \exp(T) |\Phi_{\text{ref}}\rangle = \exp(T_1 + T_2 + \dots) |\Phi_{\text{ref}}\rangle. \quad (2.9)$$

The linear excitation operator of particle-hole CI is promoted into the exponent and becomes an amplitude operator  $T$  that is again organized by particle-hole rank. A truncation of the  $T$  operator at the 2p2h level defines the coupled cluster singles-doubles (CCSD) approach. The amplitudes  $T_{ph}, T_{pp'hh'}, \dots$  contained in the  $T$  operator have to be determined from the solution of a set of coupled nonlinear equations, which results from inserting  $|\Psi_{\text{CC}}\rangle$  into the many-body Schrödinger equation and projecting on the individual basis states [44].

The resulting coupled-cluster equations can also be interpreted as a specific decoupling condition for the similarity transformed Hamiltonian

$$H_{\text{CC}} = \exp(-T)H \exp(T), \quad (2.10)$$

which schematically can be written as

$$\langle \Phi_{\text{ref}} | H_{\text{CC}} | \Phi_{\text{ref}} \rangle = E_{\text{CC}}, \quad \langle \Phi_{1ph} | H_{\text{CC}} | \Phi_{\text{ref}} \rangle = 0, \quad \langle \Phi_{2p2h} | H_{\text{CC}} | \Phi_{\text{ref}} \rangle = 0, \dots, \quad (2.11)$$

where  $|\Phi_{npnh}\rangle$  represents any of the  $npnh$  excited basis states. Thus the similarity transformation described by the wave operator  $\exp(T)$  suppresses all pieces of the Hamiltonian that couple the reference state to particle-hole excitations, i.e., the transformation decouples the reference state from particle-hole excitations.

**In-Medium Similarity Renormalization Group.** The concept of decoupling was already present in the discussion of the SRG transformation of the Hamiltonian in few-body spaces that we discussed as part of the pre-processing for an NCSM calculation. As we already emphasized, the concept of the SRG is very general and flexible and we can use it to define a stand-alone many-body method [45,46]. We use the flow equation at the  $A$ -body level and write all operators in second quantization creation and annihilation operators normal-ordered from with respect to

a single-determinant reference state  $|\Phi_{\text{ref}}\rangle$ . As a result the operator-valued flow equation

$$\frac{dH(s)}{ds} = [\eta(s), H(s)] \quad (2.12)$$

can be rewritten as a set of coupled differential equations for the matrix elements of the normal ordered Hamiltonian. All the initial normal-ordered operators as well as the commutator expressions on the right-hand-side of the flow equation have to be truncated at a relatively low particle-rank—the particle-hole or cluster truncation of the previous approaches enters the in-medium SRG through this back-door. Typically all normal-ordered terms beyond the two-body level are discarded, defining the IM-SRG(2) scheme. Three and multi-body operators are still captured at this truncation level, but only in an average sense through their normal-ordered zero, one, and two-body contributions.

Note that CI(2p2h), CCSD and IM-SRG(2) all deal with a similar number of unknowns and they are all built on some kind of two-particle truncation. Although CCSD and IM-SRG(2) also capture some specific correlations beyond the two-particle level, they do not offer the flexibility to represent all possible three-particle (and beyond) correlations. All three methods lead to a different category of numerical problem: from a matrix eigenvalue problem, a nonlinear coupled system of equations, to a coupled system of first-order differential equations.

**Valence-Space Shell Model.** Both, coupled-cluster and in-medium SRG are limited to the description of ground states of closed-shell nuclei in their basic formulation. The step towards excited states and open-shell systems requires either a nontrivial generalization of the formalism or the use of a secondary many-body method for processing the many-body decoupled Hamiltonian. One option for this secondary many-body calculation is the valence-space shell model. Both, coupled cluster and in-medium SRG can be adapted to a valence-space decoupling pattern [47–51]—starting from the closed-shell core as reference space, the matrix elements of the Hamiltonian that connect the valence states to either core or excluded states are suppressed. In this way, the Hamiltonian matrix assumes a block-diagonal form and a solution of the eigenvalue problem within the valence space is sufficient to extract the ground state and low-lying excited states.

In-medium SRG and coupled cluster provide an *ab initio* foundation for the traditional valence-space shell model as well as a practical and efficient scheme to derive a valence space Hamiltonians from a realistic free-space interaction, e.g., from chiral EFT. The range of these calculations is the same as for valence-space shell model calculations with phenomenological Hamiltonians, i.e., the computational limitations result from the shell-model diagonalization and not from the in-medium SRG or coupled-cluster calculation that defines the decoupled Hamiltonian. They also share the same limitations as the conventional shell model, e.g., when it comes to the description of collective phenomena. We will come back to this point in Section 2(e).

**Multi-Reference Approaches.** One can improve on this situation by generalizing the decoupling idea to a so-called multi-reference scenario. We do not start from a single Slater determinant as reference state, but rather a superposition of multiple Slater determinants that span the reference space. The decoupling aims to suppress all matrix elements that connect states from the reference space with the rest of the Hilbert space. The resulting Hamiltonian then serves as input for a subsequent many-body calculation that covers the reference space and extracts the relevant observables. This multi-reference generalization can be readily implemented in the in-medium SRG context, and it has been employed in different settings. One option is to use angular-momentum projected deformed Hartree-Fock-Bogoliubov states as reference space [50,52,53]. In this way, intrinsic deformation can be built into the reference space from the beginning and the decoupling takes care of particle-hole excitation on top of the intrinsically deformed reference. Another option is to use a general CI calculation in a small model space to define the reference state. In this way, all the static and dynamic correlations that are captured

in the reference space are treated exactly and the decoupling only accounts for the admixtures of high-lying excitations beyond the reference space.

**In-Medium No-Core Shell Model.** The latter scheme is the basis for the in-medium NCSM (IM-NCSM) [54]. We start from an NCSM calculation in a small model space, typically  $N_{\max} = N_{\text{ref}} \leq 4$ . The ground state obtained in this calculation defines the reference state for the multi-reference in-medium SRG decoupling. The generator is defined such that matrix elements connecting the reference space with higher-lying basis states are suppressed, i.e., we decouple the small- $N_{\text{ref}}$  reference space from the rest of the Hilbert space. The output of the multi-reference IM-SRG evolution are the matrix elements of the transformed Hamiltonian and of consistently transformed operators of all relevant observables. These matrix elements are the input for a final NCSM calculation that provides access to the observables of interest. There are three main control parameters involved in the IM-NCSM: The truncation  $N_{\text{ref}}$  for the reference NCSM calculation, the flow parameter for the IM-SRG evolution, and the  $N_{\max}$  truncation of the final NCSM calculation. All three parameters can be varied to assess the many-body uncertainties inherent to the approach, mainly because of the truncation of the multi-reference IM-SRG evolution at the normal-ordered two-body level. Because of the decoupling of the reference space, the final NCSM calculation is essentially converged at  $N_{\max} \approx N_{\text{ref}}$  if the target states are well represented in the initial reference space. Note that with growing  $N_{\text{ref}}$  the reference space covers more of the relevant Hilbert space and the decoupling has less effect. Thus, despite the truncation of the IM-SRG to normal-ordered two-body operators, the precision of calculation systematically improves with increasing  $N_{\text{ref}}$  and becomes formally exact in the limit  $N_{\text{ref}} \rightarrow \infty$ . The option to vary or design the reference space according to the specific structure of the problem is a great advantage of multi-reference approaches. This will become particularly important for the description of electromagnetic observables, as discussed later.

#### (d) Present status

Ab initio nuclear structure theory with all the ingredients discussed in the preceding sections has reached a remarkable level of maturity in a relatively short amount of time.

Today we have different families of NN+3N interaction from chiral EFT available that serve as a universal starting point for a wide range of ab initio methods and applications. The differences in the available sets of interaction lie in the choice of regulator scheme and scale, the available range of chiral orders, and the way the low-energy constants are fit to data from few or many-body systems. Most interactions rely on a chiral EFT formulation with explicit nucleon and pion degrees of freedom, while some also include intermediate delta excitations. While the latter are typically limited to next-to-next-to-leading order (N2LO) in the chiral expansion for the NN and 3N interaction [55], the former reach order N4LO and beyond for the NN interaction [56–58] and order N3LO for the 3N interaction. Moreover, the full sequence of chiral orders from LO to the maximum order, e.g., N3LO, is available and allows for a direct investigation of the convergence of the chiral expansion at the level of observables [59–61]. In addition the convergence pattern of observables can be used to quantify uncertainties of the observables resulting from the truncation of the chiral expansions for the interaction and sophisticated Bayesian schemes have been developed for this purpose [15,16,61,62].

All state-of-the-art chiral interactions reproduce ground-state energies of light and medium mass nuclei in good agreement with experiment. Obviously, ground-state energies are the first benchmark when assessing the performance of new chiral interactions as well as new many-body methods. Systematic benchmark calculations employing different many-body methods with the same chiral NN+3N Hamiltonian have played an important role in validating ab initio methods and assessing their uncertainties.

The next ground-state observables typically studied after the energies are root-mean-square (rms) radii. For all of the early chiral NN+3N interactions, there are systematic deviations of the calculated point-proton rms radii in the medium-mass regime compared to experiment. Only the

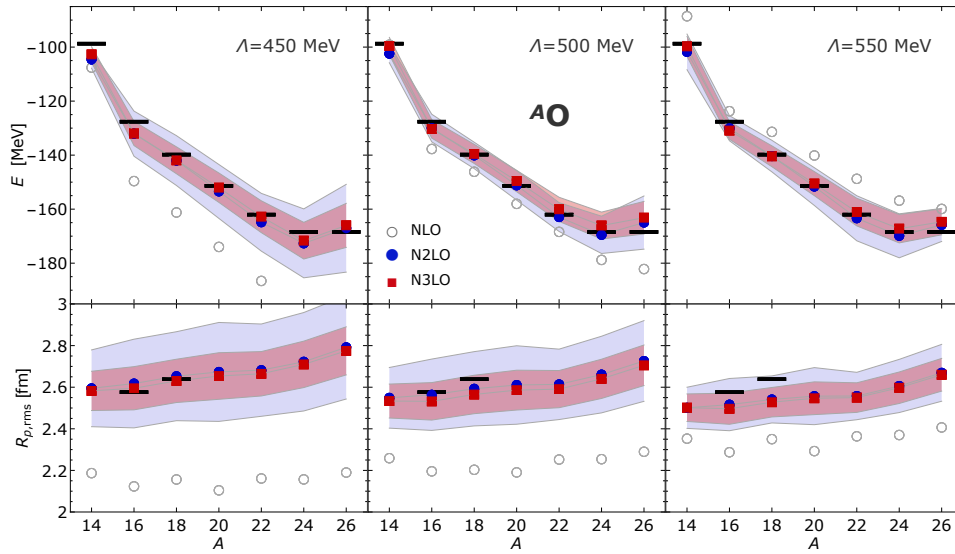


**Figure 2.** Ground-state energies (top row) and point-proton rms radii (bottom row) of the even oxygen isotopes obtained in the IM-NCSM using chiral NN+3N interactions up to N3LO with non-local regulators and different cutoffs  $\Lambda$ . The uncertainty bands included for N2LO and N3LO indicated the combined many-body and interaction uncertainties. Figure adapted from [63], see [59] for more details.

most recent generation of chiral NN+3N interactions has resolved this problem, however, the detailed understanding of the source of this discrepancy is still missing [59]. An example of the performance of recent chiral NN+3N interactions for the description of ground-state energies and point-proton rms radii is shown in Figure 2 for the oxygen isotopic chain. The panels show the ground-state energy and the point-proton rms radii obtained in the IM-NCSM for a family of non-local NN+3N interactions from NLO to N3LO with three different values of the regulator cutoff  $\Lambda$ . Based on the order-by-order behavior of the observables, uncertainties due to the chiral truncation are estimated. The combination of those interaction uncertainties with the many-body uncertainties assessed via a variation of the IM-NCSM truncations, as discussed earlier, leads to the uncertainty bands depicted for N2LO and N3LO. Within these theory uncertainties, we observe a robust agreement of the calculated ground-state energies with experiment. Also the radii are in good agreement with experiment, particularly for the two lower cutoffs. The agreement of the radii was a major problem in previous generations of chiral interactions.

Going beyond the ground-state, the excitation energies are the next target of interest. As discussed earlier, for many of the medium-mass approaches this step requires extensions of the method, often leading to a hybrid scheme such as the valence-space shell model with Hamiltonians from a coupled-cluster or IM-SRG decoupling. For NCSM-type methods, including the IM-NCSM, the excitation spectrum is obtained without extra effort and on the same footing as the ground state. Comparisons of excitation spectra obtained in *ab initio* calculations with experimental data typically show a good agreement. Some excited states, however, might exhibit a problematic convergence behaviour, e.g., because of prominent intrinsic  $\alpha$ -clustering, which is difficult to capture in many-body expansions build on a spherical basis. Another limitation is the coupling to the continuum, which becomes relevant once the first particle-separation threshold is approached. The proper inclusion of continuum degrees of freedom requires significant extensions of the many-body framework, which we do not address here.

### (e) Challenges of electromagnetic observables

The previous discussion shows that *ab initio* theory has come a long way for the description of ground-state energies and radii as well as the excitation spectrum. The natural next step is the description of electromagnetic observables, thus, addressing the full spectroscopy of low-lying states. This step is challenging, for a number of different reasons. Already from a general physics point of view, we expect electromagnetic observables to probe the structure of the nucleus in a different and more subtle way than, e.g., binding energies. Depending on their multipolarity, they depend sensitively on the spin and angular momentum structure of the nucleus and, in some cases, also on the long-range behavior of the nuclear wave functions. On the one hand, this is a desired aspect, since it provides us with a more comprehensive and detailed picture of the structure of nuclei. On the other hand, it poses new problems for precise *ab initio* calculations of these observables.

**No-Core Shell Model.** The NCSM provides direct access to the excited states through the solution of the Schrödinger equation as a matrix eigenvalue problem. Therefore, all expectation values and transition matrix elements involving excited states can be readily computed. As specific examples we consider the magnetic dipole (M1) operator and the electric quadrupole (E2) operator, and the associated moments and reduced transition strengths. The majority of existing calculations on electromagnetic properties of nuclei start from the simplest possible one-body form of electromagnetic multipole operators. However, when approaching these observables from an *ab initio* perspective, two complications have to be considered.

First, since we typically use a Hamiltonian that is pre-processed through a free-space SRG evolution, all other operators that are used in conjunction with the eigenstates have to undergo a consistent SRG transformation. As discussed earlier, such a unitary transformation induces many-body terms beyond the particle-rank of the initial operator. If we use a simplistic one-body form for the multipole operators, they will acquire two-body and multi-body contributions induced by the SRG transformation. These contributions have to be included in the calculation to maintain the unitary equivalence with the original many-body problem. For the induced two-body part this is rather straight forward, but for three- and multi-body contributions this becomes computationally challenging since we are dealing with non-scalar operators.

Second, the chiral EFT framework for constructing the nuclear interactions provides the means for a consistent construction of two-body corrections to the electromagnetic multipole operators based on two-body current and charge-density contributions. The inclusion of these correlations allows for a fully consistent description of electromagnetic observables based on chiral EFT. The simple single-particle form of electromagnetic multipole operators only constitutes the leading-order contribution to this chiral expansion.

At present, these two aspects are rarely taken into account in *ab initio* calculations beyond the few-body domain. An example for the inclusion and study of both aspects are the precision NCSM calculations for M1 observables in  ${}^6\text{Li}$  reported in Ref. [64]. This is a particularly well suited system for a precision NCSM study. First of all,  ${}^6\text{Li}$  is sufficiently light so that NCSM for relatively large  $N_{\text{max}}$  truncation parameters are possible. Second, the M1 observables typically show a robust convergence pattern, since the M1 operators only probe the spin and angular momentum structure of the system, which can already be captured in NCSM model spaces of moderate size. Therefore, the many-body uncertainties resulting from the model-space convergence of the observables are well under control and we can focus on the influence of chiral two-body currents and the consistent SRG evolution. Figure 3(a) illustrates these effects for the ground-state magnetic dipole moment  $\mu(1^+)$  and the  $B(M1, 0^+ \rightarrow 1^+)$  transition strength from the excited  $0^+$  state to the  $1^+$  ground state for four different chiral NN+3N interactions. The error bars at the individual data points indicated the NCSM convergence uncertainties. One set of calculations uses the simple single-particle form of the M1 operator, which constitutes the leading order in the chiral expansion, without a consistent SRG transformation — most NCSM calculations of electromagnetic properties in the past have been performed at this level. The second set of

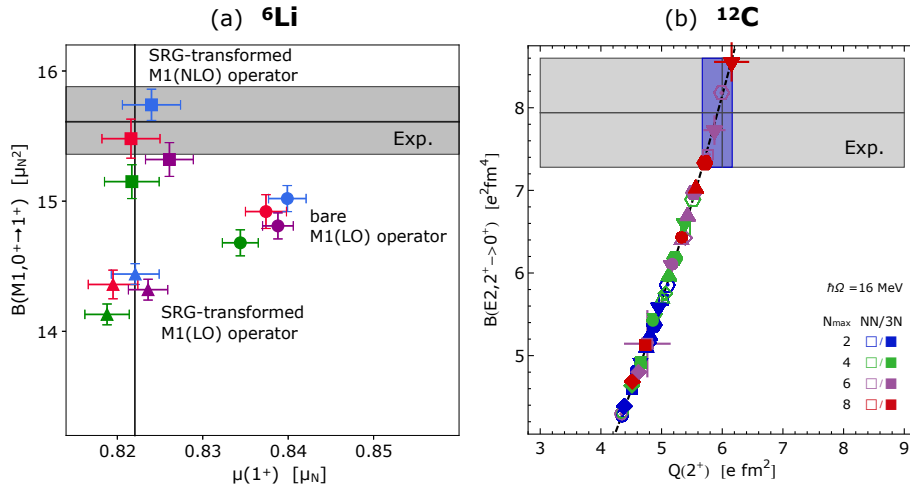


**Figure 3.** (a) NCSM calculations for the magnetic dipole moment  $\mu(1^+)$  and the transition strength  $B(M1, 0^+ \rightarrow 1^+)$  involving the  $0^+$  excited state and the  $1^+$  ground state in  ${}^6\text{Li}$ . The different colors show different chiral NN+3N interactions. The different groups of symbols correspond to calculations with the the bare M1 operator at LO, the SRG-transformed M1 operator at LO, and the SRG-transformed M1 operator a NLO, respectively. Figure adapted from [64]. (b) NCSM calculations for the quadrupole moment  $Q(2^+)$  and the transition strength  $B(E2, 2^+ \rightarrow 0^+)$  involving the  $2^+$  excited state and the  $0^+$  ground state in  ${}^{12}\text{C}$ . Here, NCSM results for different chiral interaction and model space truncation  $N_{\text{max}}$  predict a strong correlation between the two observables, but, due to incomplete convergence, do not yield a specific values. Figure adapted from [65].

calculations uses the M1 operator at LO but account for its SRG transformation at the two-body level. The third set of calculations includes the chiral two-body corrections to the M1 operator at NLO and the consistent SRG transformation. First of all, we observe that the many-body and interaction uncertainties for this observable are well under control, i.e., the error based and the scatter for the four different interactions are small and of similar size. Therefore, the small effects of the SRG transformation, which changes the  $B(M1)$  by about 5% and  $\mu$  by about 2.5% are relevant. Similarly, the effect of the two-body current contributions to the M1 operator are visible, they change the  $B(M1)$  by about 8% and have very little effect on  $\mu$ . This last step brings the calculation into excellent agreement with the high-precision experiment. Thus, for M1 observables we are in the position to perform precision studies with well controlled uncertainties.

For E2 observables, the situation is much more difficult. In principle, the chiral two-body current contributions to the E2 operator and the consistent SRG evolution have to be considered as well. However, the major source of theory uncertainties in this case is the model-space convergence of E2 observables, which is much worse than for M1 observables. Already in its leading-order or single-particle form, the E2 operator probes the angular momentum structure of the nuclear states as well as the long-range behavior of the wave functions. This leads to a significantly slower convergence compared to, e.g., energies. Therefore, model-space truncations are the dominant limitation in all types of ab initio calculations of E2 observables.

In the NCSM, the situation is rather well controlled since we only deal with  $N_{\text{max}}$  as single truncation parameter. However, for mid-p-shell nuclei we are not able to provide converged NCSM calculations for electric quadrupole moments or transition strengths. As an example we consider  ${}^{12}\text{C}$  and the E2 transition from the first  $2^+$  state to the ground state as well as the quadrupole moment of the  $2^+$  state. Within the range of  $N_{\text{max}}$  truncations that is computationally accessible, no complete convergence can be obtained for these observables. Moreover, model-space extrapolations of these observables are very difficult and introduce large uncertainties [66].

One way to extract meaningful information on E2 observables despite the incomplete convergence is to exploit correlations among different observables. Even non-converged many-body calculations might reveal such correlations and can be used to extract precise and accurate values for one observable based on a known experimental value for a second, correlated observable. An example for the application of such a scheme is the quadrupole moment  $Q$  of the first excited  $2^+$  state in  $^{12}\text{C}$ . Ab initio NCSM calculations show a strong correlation of this quadrupole moment with the  $B(E2)$  transition strength to the ground state. Irrespective of the  $N_{\text{max}}$  truncation parameter and the specific chiral interaction used, all calculations fall onto a well-defined line in  $Q$ - $B(E2)$ -plane, as shown in Figure 3(b). Note that this include very small NCSM model spaces, e.g.,  $N_{\text{max}} = 2, 4$  which are far from convergence. For a given interaction at the specific  $\hbar\Omega$  value shown here, both,  $Q$  and  $B(E2)$  increase with increasing  $N_{\text{max}}$  and, thus, move upwards along the correlation line.

The correlation can be nicely parametrized by a modified rotor model, as discussed in Ref. [65]. With the experimentally well known value for the  $B(E2)$  transition strength and using the correlation predicted by the ab initio NCSM we can extract a value for the quadrupole moment that is much more precise than any extrapolation of the NCSM results could. Similar correlations have also been identified for pairs of other observables, e.g., the charge radius and the quadrupole moment [67].

**Medium-Mass Methods.** Given the difficulties with converging E2 observables in the NCSM, one might think that many-body schemes that cover larger single-particle spaces are advantageous. Medium-mass methods, such as coupled-cluster and the in-medium SRG, fall into the categories of many-body approaches which can access large single-particle spaces, however, they have to use an additional truncations with respect to the particle rank of the excitations or operators.

In order to address electromagnetic observables in these approaches, we have to go beyond the ground state of closed-shell nuclei. One option are valence-space calculations, where coupled-cluster or in-medium SRG are used to construct a valence-space interaction for a subsequent shell-model diagonalization. As discussed earlier, the decoupling transformation has to be applied not only to the Hamiltonian, but to all observables consistently. Thus, in the case of electromagnetic observables, the electromagnetic multipole operators get modified by the transformation. This modification is important—since the decoupling transformation drastically simplifies the many-body states and thus eliminates correlations, the transformation of the operators has to compensate for this. There is some analogy to phenomenological effective charges in the traditional shell model, which also simulate the effect of missing correlations by limiting the problem to a small valence space. However, there are important differences as well. There is no phenomenology in the consistent transformation of electromagnetic operators in the decoupling approaches—the transformed operators are completely determined by the decoupling procedure and there are no free parameters. Furthermore, the transformation changes the structure of operators significantly. When starting from the simplistic one-body electric or magnetic multipole operators, the transformation will induce two-, three- and multi-body contributions to these operators. Unlike effective charges, which amount to a simple scaling of the one-body operators, the consistent transformation leads to a much more complicated operator structure with contributions for all particle ranks. This complexity at the level of the operators is necessary to capture all the multi-particle correlations that are eliminated from the many-body states by the decoupling transformation.

At this point a problem emerges: In practical calculations we cannot include all the many-body contributions generated by the transformations, neither for the Hamiltonian nor for the electromagnetic operators. In most practical calculations all operators are truncated at the (normal-ordered) two-body level. This approximation is acceptable as long as the contributions of the higher-rank operators is below the desired precision of the calculation. For simple observables like energies or radii, this is often the case. However, for electromagnetic operators this can

cause problems and once again E2 observables are a particularly difficult case. This has been analyzed in Ref. [68] in detail for the valence-space calculations coupled with the IM-SRG. Generally, the E2 observables connected to collective effects, e.g., intrinsic deformation, are strongly underestimated in the truncated calculations.

This problem is not limited to the valence-space-version of the IM-SRG, it also appears in multi-reference IM-SRG approaches such as the IM-NCSM. An intrinsic advantage of the multi-reference approaches is the flexibility to choose the reference space. Since all correlations that can be represented in the reference space are treated explicitly and are not subject to the decoupling, the choice of the reference space provides an extra level of control. Simply speaking, if the reference space captures all the relevant correlations for the description of a specific electromagnetic observable, then the decoupling will not affect this observable too much.

In Figures 4 and 5 we provide a summary of results obtained in the IM-NCSM for the even carbon isotopes from  $^{10}\text{C}$  to  $^{20}\text{C}$ . The left-hand panels provide an overview of the systematic behaviour of the ground-state energy, the excitation energy of the first  $2^+$  state, the  $B(E2)$  transition strength from the first  $2^+$  to the ground state, and the quadrupole moment of the first  $2^+$  state throughout the chain. The right-hand panel shows the excitation spectra for the different isotopes.

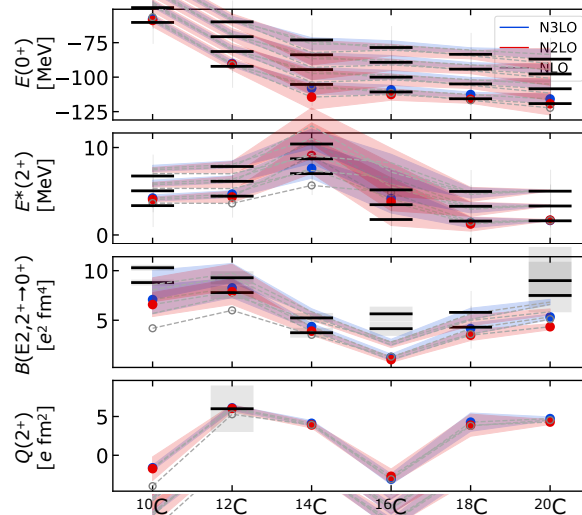


**Figure 4.** Summary of the ab initio IM-NCSM results for the ground-state energy, the  $2_1^+$  excitation energy, the  $B(E2, 2_1^+ \rightarrow 0_1^+)$  transition strength, and the quadrupole moment  $Q(2_1^+)$  for the even carbon isotopes from  $^{10}\text{C}$  to  $^{20}\text{C}$  using non-local chiral NN+3N interactions up to N3LO. The bands indicate the theory uncertainties. The adopted experimental values [69] are also presented, where known. Newer experiments are discussed below (see, e.g., section 3(a)).

### 3. Experimental efforts to guide the theoretical developments

The theoretical developments have to be confronted with experimental investigations that deliver key spectroscopic information on isotopic chains accessible to well-established ab initio approaches as well as new medium-mass methods. As described above, a prediction extracted from an ab initio calculation is subject to a number of different choices and truncations, from the many-body methods themselves to the formulation of the chiral EFT interactions that are employed.

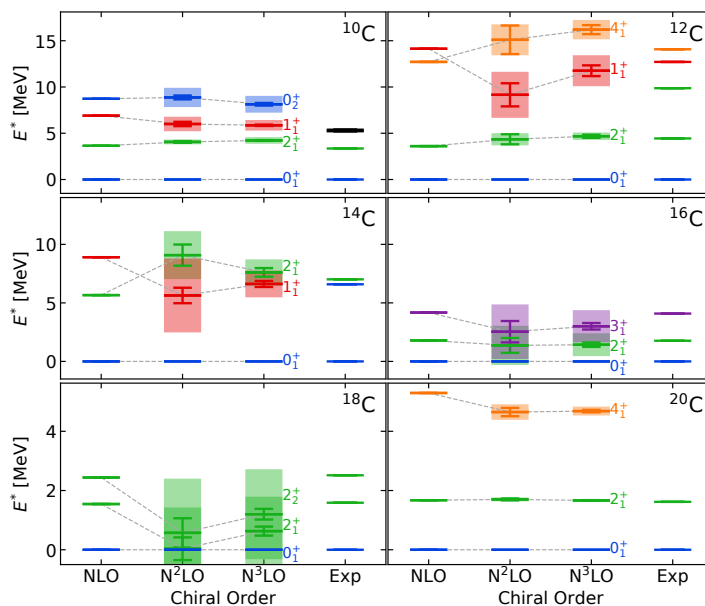


**Figure 5.** Excitation spectra obtained in the ab initio IM-NCSM for the even carbon isotopes from  $^{10}\text{C}$  to  $^{20}\text{C}$  using non-local chiral NN+3N up to N3LO compared to experiment. The bands indicate many-body uncertainties and the error bars the chiral interaction uncertainties.

An ideal experimental arena for the refinement of the theory, especially in its effort to extend its applicability to heavier systems, is the carbon and oxygen isotopic chains. These nuclei can serve as a benchmark for testing chiral EFT interactions used in well-established ab initio approaches (e.g., NCSM, GFMC) by measuring for the first time or with improved accuracy properties that are sensitive to the underlying interaction. At the same time, these isotopic chains allow for test of new medium-mass approaches (e.g., IM-SRG), which start to become competitive in this mass region. The carbon and oxygen isotopic chains occupy a unique position in the hierarchy of ab initio methods—they are at the upper end of the domain of applicability of quasi-exact methods like the NCSM and at the lower end of the domain, where medium-mass methods provide sufficiently accurate results<sup>1</sup>. From the experimental perspective, these isotopic chains can be studied up to the (proton and neutron) driplines and can provide a wealth of experimental information, avoiding additional complications of coupling to the continuum as is the case for lighter systems. Therefore, this specific region of the nuclear chart provides unique opportunities for precision tests of different types of ab initio approaches.

In this section we focus our attention on selective experimental efforts to extract E2 observables, which have been highlighted as notoriously difficult quantities to be described by ab initio theory (see section 2(e)), along the carbon and oxygen isotopic chains. There are two fronts that need to be addressed experimentally. The precision frontier, for transitions that were known experimentally but not to an accuracy that would allow any meaningful comparison with ab initio calculations, and the discovery frontier, measuring E2 matrix elements in key nuclei for the first time.

The experimental cases that are presented in this contribution are not exhaustive (see, e.g., [70–74]), however, they have emerged from the cultivation of robust synergies between the experimental and theoretical activities over numerous years, which is the essence of this contribution.

<sup>1</sup>Note that for lighter systems, additional truncations typically used in the medium-mass methods, e.g., the normal-ordered two-body approximation of three-body contributions, lead to larger relative uncertainties.

## (a) The $2^+$ state of $^{12}\text{C}$ and its spectroscopic quadrupole moment

Electromagnetic diagonal matrix elements  $\langle I || \hat{O}_\lambda || I \rangle$  are very sensitive to the details of the nuclear wavefunction, as they depend on the one state that is being investigated describing transitions between magnetic sub-states. Experimentally these can be accessed for example through the spectroscopic quadrupole moment  $Q_s$ . The influence of the diagonal matrix element is important in low-energy Coulomb excitation and is due to second-order transitions between magnetic sub-states, the so-called re-orientation effect, which results in the sensitivity of the Coulomb excitation cross section to the quadrupole moment.

Although measurement of the  $Q_s(2^+)$  in several carbon isotopes would be highly desirable, see, e.g., Figure 4 and the variability of this observable along the carbon isotopic chain, the difficulty of extracting carbon (and in general light) isotopes as low-energy and high-purity radioactive ion beams (RIB) with sufficient intensity, makes  $^{12}\text{C}$  the only candidate for studying experimentally the  $Q_s(2^+)$  in this isotopic chain presently. In the future, this would be possible in state-of-the-art radioactive-ion-beam facilities that are being developed now, e.g., the re-accelerated exotic ion beams at the FRIB facility [75] will offer unique opportunities to perform such experiments.

Figure 6(a) summarizes the experimental results to date of the spectroscopic quadrupole moment of the  $2^+$  state of  $^{12}\text{C}$  and how they compare with theory. The high energy of the  $2^+ \rightarrow 0^+$   $\gamma$ -ray transition (4.44 MeV) and the low Coulomb-excitation cross section make this a very challenging measurement, reflected in the limited number of experiments that have attempted this measurement [76–78]. It is interesting that the ab initio calculations [65,79–81] firmly predict  $Q_s(2^+) \approx +6 \text{ efm}^2$ . This lies at the very edge (within  $2\sigma$ ) of the experimental value.

When trying to benchmark the theoretical predictions, it is important to consider also the calculated  $B(E2)$  transition strength, and the dimensionless ratio  $B(E2)/Q_s^2$ , which offers an appealing indicator to extract structural information on even-even nuclei [82]. This ratio is important to assess any convergence limitations that the ab initio calculations face given the sensitivity of the E2 operator to the long-range behaviour (tails) of the wavefunctions involved. In fact, several studies [65,83,84] have shown the robustness of this ratio, that converges faster than the two observables individually. The comparison in Figure 6(b) could suggest that the microscopic interactions need to be revisited, if, to some extent, the ratio minimizes the convergence issues.

## (b) The puzzle of $^{16}\text{C}$

Large-scale no-core shell model (NCSM) calculations, starting from realistic Hamiltonians without adjustable parameters or effective charges, have been performed for low-lying states of even-even carbon isotopes with  $A=10\text{--}20$  (see [66] and Figure 4) in order to understand their structural evolution with increasing neutron number. In these calculations two striking features have been observed; the quadrupole moment of the first  $2^+$  state in  $^{16}\text{C}$  is negative, unlike for all other neutron-rich carbon isotopes, and the electromagnetic transition strengths exhibit a strong sensitivity to the details of the nuclear interaction.

In particular, a strong suppression of the  $2_2^+ \rightarrow 0_{g.s.}^+$  transition has been predicted when the 3N interaction is included. Indeed, the  $2_2^+ \rightarrow 0_{g.s.}^+$  transition strength is suppressed by a factor of  $\approx 7$  in the calculation with the chiral 3N compared to chiral NN only. At the same time the CD-Bonn potential, a well-tested NN interaction constructed within meson exchange theory and very successful in the description of p-shell spectroscopy, predicts a transition strength larger by a factor of  $\approx 20$  than the chiral NN+3N interaction. In addition, a 40% change in the size of the quadrupole moment of the first  $2^+$  state is observed when using the chiral 3N interaction, as opposed to 2N interactions.

An early experimental study of  $^{16}\text{C}$  [88] points to the inclusion of 3N forces in order to reproduce the experimental branching ratios of the  $2_2^+ \rightarrow 2_1^+$  and  $2_2^+ \rightarrow 0_{g.s.}^+$  transitions that have been constrained to  $>91.2\%$  and  $<8.8\%$ , respectively. Since then, further experiments have been

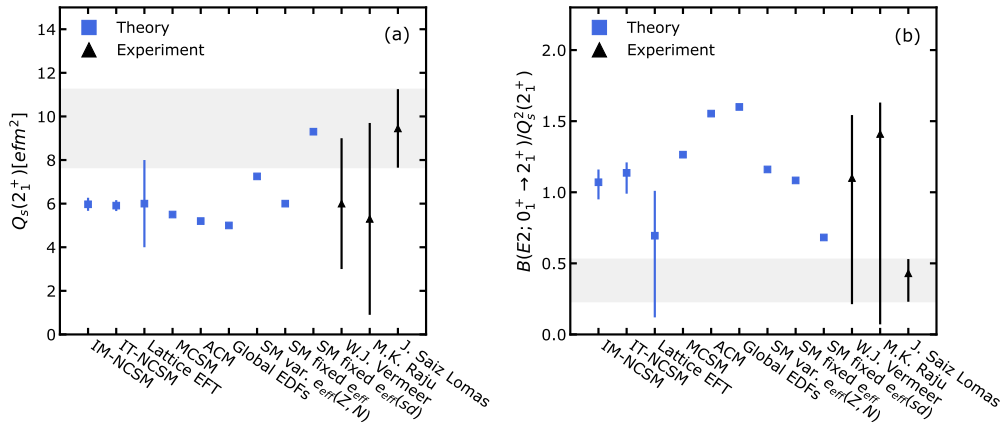


**Figure 6.** (Color online) Theoretical (blue filled squares) and experimental values (black filled triangles) for the (a)  $Q_s(2_1^+)$  and (b) dimensionless ratio  $B(E2; 0_1^+ \rightarrow 2_1^+)/Q_s^2(2_1^+)$  of  $^{12}\text{C}$ . From the left to the right: In Medium - No Core Shell Model (IM-NCSM) and Importance Truncated - No Core Shell Model (IT-NCSM) using 2- (NN) and 3-body (3N) (NN+3N) chiral Effective-Field-Theory (EFT) interactions [65,79], lattice EFT at Leading Order (LO) [80], no-core ab initio Monte Carlo Shell Model (MCSM) using the Daejeon16 interaction [81], Algebraic Cluster Model [85], global Energy Density Functionals [86], Shell-Model calculations using variable and fixed effective charges ( $e_{eff}$ ) [87], experimental values measured by Vermeer *et al.* [76], Raju *et al.* [77] and Saiz Lomas *et al.* [78]. The shaded area follows the experimental values from the most recent experiment which delivered the most precise value to date for the  $Q_s(2_1^+)$  [78]. The figure is modified from [78].

performed with the goal to measure transition strengths in  $^{16}\text{C}$  and shed light on the role of 3N forces in the structure of this nucleus, see [74] and [89]. The work from [74] gives only a lower lifetime limit for the  $2_2^+$  of  $^{16}\text{C}$ , not sufficient to confront modern ab initio calculations. The work of [89], however, delivers a robust constraint to the lifetime of the  $2_2^+$  of  $^{16}\text{C}$ , which can be translated into individual constraints for the three transitions dominating the de-excitation of the  $2_2^+$  state of  $^{16}\text{C}$ , i.e.,  $B(E2; 2_2^+ \rightarrow 2_1^+)$ ,  $B(M1; 2_2^+ \rightarrow 2_1^+)$ , and  $B(E2; 2_2^+ \rightarrow 0_{g.s.}^+)$ , see Figure 7.

No-Core Shell-Model calculations using state-of-the-art chiral NN+3N interactions at N3LO for both the NN and the 3N contributions and a generalized natural-orbital basis (instead of the conventional harmonic-oscillator single-particle basis) reproduce, for the first time, the experimental findings remarkably well [90]. This is a clear demonstration of how theory advances are triggered by challenging experimental results in a close, constructive interaction between theory and experiment.

### (c) The $2^+$ state of $^{20}\text{C}$ and its lifetime

The spectroscopy of very neutron-rich systems is more sensitive to the neutron-neutron interaction as well as the three-neutron interaction (T=3/2 isospin channel), which is currently a frontier in the physics of nuclei for shell structure and its evolution to the driplines. Constraining the neutron 3N interaction in chiral EFT has far-reaching implications beyond the physics of exotic nuclei. 3N forces play a very important role in neutron stars and pure neutron matter, the latter being a natural bridge between astrophysical observation of neutron stars and terrestrial nuclear experiments.  $^{20}\text{C}$ , with proton-neutron asymmetry  $N/Z=2.3$ , is the most asymmetric nucleus for which lifetime measurements can be performed, enhancing effects of the T=3/2 isospin channel in the 3N interaction.

Given that E2 observables provide an excellent testing ground for chiral interactions and many-body methods that goes beyond the aspects probed by the excitation energies alone, it is of the utmost importance to pin down the lifetime of the  $2^+$  state of  $^{20}\text{C}$  with high accuracy

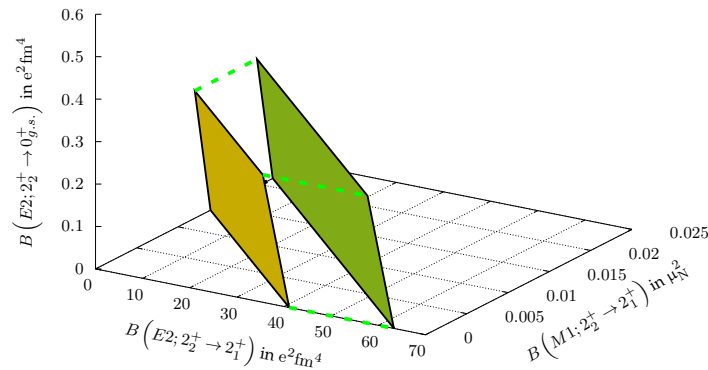


**Figure 7.** Constraints to the three transition depopulating the  $2_2^+$  state of  $^{16}\text{C}$  as extracted in [89]. The calculated transition strengths should lie within the volume created by the two rectangles.

and precision. Results from In-Medium NCSM calculations with a consistent N3LO NN+3N interaction for excitation energies,  $B(E2)$  and  $Q(2^+)$  for  $^{20}\text{C}$  are shown in Figure 4 together with the experimentally adopted value<sup>2</sup>. It is clear that from an experimental perspective the data should be of the highest quality and accuracy for any meaningful comparison with theory. Therefore new experiments should be designed with an aim of delivering a confirmation of the accepted value and a reduction of the associated error bars.

$^{20}\text{C}$  can be accessed experimentally for spectroscopy in fragmentation facilities. The RIBF facility at the Nishina Centre, RIKEN (Japan) [93] and the FRIB facility (USA) [75] are uniquely positioned to deliver a high precision measurement of the lifetime of the first excited state in  $^{20}\text{C}$ . The capability of these facilities to deliver high-intensity radioactive ion beams coupled to state-of-the-art  $\gamma$ -ray detection arrays, such as GRETA/GRETINA [94] and the future HYPATIA array [95], enables detailed spectroscopy of  $^{20}\text{C}$ , a critical benchmark for ab initio developments.

#### (d) The neutron-rich oxygen isotopes, $^{21,22}\text{O}$

Neutron-rich oxygen isotopes are an ideal playground for testing ab initio theory, lying at the interface of the light- and medium-mass regions. Indeed, these isotopes can be treated in quasi-exact methods, such as extensions of the no-core shell model (NCSM), while due to their semi-magic nature, having a closed proton shell at  $Z=8$ , they are accessible to many-body approaches that can be applied to heavier systems. First valence-space calculations with NN+3N forces were able to explain for the first time the so-called oxygen anomaly, i.e., the location of the oxygen dripline at  $^{24}\text{O}$  [96]. More recently, large-space ab initio calculations have confirmed those early results [52,97,98] treating all nucleons as explicit degrees of freedom and have extended dripline predictions to the entire region [99]. Excitation spectra in oxygen isotopes have also been obtained with NN+3N forces, generally yielding agreement with experiment [48,49,100,101]. A critical next step is to benchmark ab initio theory against electromagnetic observables, with a particular focus on E2 transition strengths.

<sup>2</sup>In the case of  $^{20}\text{C}$ , there are only two measurements available for the  $B(E2; 2^+ \rightarrow 0^+)$  [91,92], which are in disagreement. However, the more recent work from [91] represents the adopted value.

A first experimental study to extract lifetimes of excited states in  $^{21}\text{O}$  was performed at the National Superconducting Cyclotron Laboratory of Michigan State University [102]. This isotope, with a neutron coupled to a  $^{22}\text{O}$  core, yielded varying results for the  $B(E2; 1/2^+ \rightarrow 5/2^+)$  transition strength for different chiral NN+3N interactions calculated using the IM-NCSM approach, demonstrating the sensitivity of the 3N forces to spectroscopic observables such as level lifetimes. Figure 8 demonstrates beautifully how theoretical calculations can be confronted by the experiment.

To further guide theory, a new experiment to measure the lifetimes of the higher excited states in  $^{21}\text{O}$  is planned to be performed at the ATLAS facility of the Argonne National Laboratory [103]. A complete experimental picture for the transition strengths in  $^{21}\text{O}$  will be delivered, and will serve as a critical benchmark for the development of the ab initio frontier.

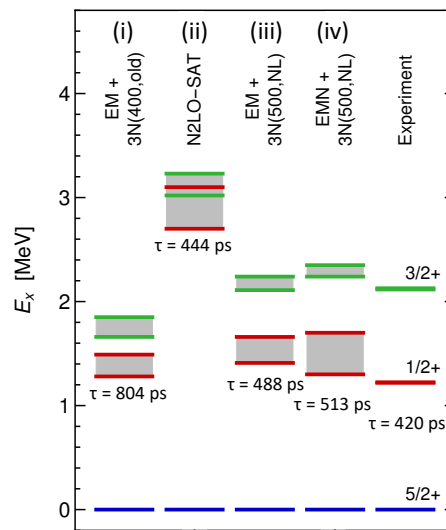


**Figure 8.** IM-NCSM calculations with four different chiral NN+3N interactions for the low-lying structure of  $^{21}\text{O}$  to assess their sensitivity to the input Hamiltonian: (i) the  $\text{N}^3\text{LO}_{\text{EM}} + \text{N}^2\text{LO}_{\text{L},400}$  interaction using the NN force of [104] in combination with a local 3N interaction at  $\text{N}^2\text{LO}$  with reduced cutoff [105]; (ii) the  $\text{N}^2\text{LO}_{\text{SAT}}$  interaction [106]; (iii) the  $\text{N}^3\text{LO}_{\text{EM}} + \text{N}^2\text{LO}_{\text{NL},500}$  with the same NN force but an updated 3N interaction with a nonlocal regulator; and (iv) the  $\text{N}^4\text{LO}_{\text{EMN}} + \text{N}^2\text{LO}_{\text{NL},500}$  with a recent NN interaction at  $\text{N}^4\text{LO}$  [56] plus a 3N interaction at  $\text{N}^2\text{LO}$  with nonlocal regulator. The lifetime of the first excited state ( $1/2^+$ ) is noted for both experimental results and theoretical calculations [102]; the theoretical  $\tau_{1/2^+}$  is calculated using the experimental transition energy.

Another critical experimental step is to reach  $^{22}\text{O}$  and study transition strengths in the last oxygen isotope where such information can be delivered experimentally. Indeed,  $^{23,24}\text{O}$  have no bound excited states, while no bound oxygen isotope can be formed beyond  $^{24}\text{O}$ . The  $B(E2; 2^+ \rightarrow 0^+)$  value of  $^{22}\text{O}$  has been measured only once before in a model-dependent way yielding large uncertainty [107]. This precision is not sufficient to discriminate between different calculations and calls for an improved measurement. A model-independent measurement of the  $B(E2; 2^+ \rightarrow 0^+)$  of  $^{22}\text{O}$ , via measuring the lifetime of the  $2^+$  state of  $^{22}\text{O}$ , can provide critical experimental information to guide the development of theory towards the drip lines.

The expected lifetime for the  $2^+$  state of  $^{22}\text{O}$  spans from  $\tau \approx 600$  fs [107] to  $\tau \approx 2$  ps; the latter value for the lifetime arises from arguments on reduced effective charges as discussed in [102]. For this lifetime range, a measurement of the lifetime of the  $2^+$  of  $^{22}\text{O}$  can be performed at a fragmentation facility, e.g., Coulomb exciting a secondary  $^{22}\text{O}$  radioactive ion beam and using

a very sensitive  $\gamma$ -ray spectrometer, such as GRETA/GRETINA [94,108] at the FRIB facility, to detect the emitting  $\gamma$  rays. Another novel way to experimentally reach  $^{22}\text{O}$  and study lifetimes of its excited states is by using a  $^{10}\text{Be}$  radioactive target and perform a Doppler-Shift Attenuation Method experiment at a low energy facility that can deliver a  $^{14}\text{C}$  radioactive beam [109]. Indeed, excited states in  $^{22}\text{O}$  can be populated through a fusion-evaporation reaction of a  $^{14}\text{C}$  beam on the  $^{10}\text{Be}$  target. The development of a radioactive  $^{10}\text{Be}$  target is currently under way [110–112] and could open up the way for low-energy experiments to study very neutron-rich light nuclei.

## 4. Future developments

The advances in ab initio theory have been pushing the mass frontier from the p-shell into the medium-mass regime. Efforts are ongoing to extend the ab initio reach into the regime of heavy nuclei. While first calculations typically target ground-state energies as simplest possible observables, the extension to the full suite of nuclear structure observables has become more important recently as a second frontier in ab initio theory. Once a specific observable can be calculated, the quest to improve the precision of the ab initio prediction represents the next frontier. For electromagnetic observables in particular, all ab initio methods are working towards this precision frontier. For some observables, such as M1 transitions and moments, precision calculations are possible today and reveal the role of two-body current contributions of chiral EFT when compared to precision experiments. Here we already see the synergy of precision experiments and theory in action. As we have discussed in detail, E2 transitions and moments pose particular challenges, e.g., in terms of model-space convergence or sensitivity to other truncations. Here, methodological improvements are still needed in order to reach the reliability and precision that ab initio methods have already achieved for simple observables like ground-state energies.

On the experimental side, we are still facing challenges in extracting key spectroscopic information in the interface of the light- to medium-mass regime, as has been already discussed in the particular cases presented in Section 3. For example, measurement of spectroscopic quadrupole moments of excited states are not currently possible in the carbon isotopic chain due to the unavailability of low-energy radioactive beams with sufficient intensity. Such experimental data would be extremely helpful for constraining ab initio calculations of the quadrupole moments (cf. Figure 4), particularly for structurally challenging cases like  $^{16}\text{C}$ . For very neutron-rich oxygen isotopes, e.g.  $^{22}\text{O}$ , where properties of the interaction at extreme isospin are probed, information on lifetimes of excited states can be delivered with the development of innovative approaches, such as the use of radioactive targets. The development at the same time of very sensitive detection systems [94,95] and new techniques, e.g. [113], are critical in enabling measurements of lifetimes of excited states. Experiments on medium-mass nuclei, e.g., [114,115], and extensions to other electromagnetic operators, e.g., M3 transitions [116], will be critical in pushing the theoretical advances further.

Moving in parallel with the theoretical developments towards the prediction of heavier (and far from stability) nuclei, the availability of radioactive-ion beams is another critical aspect of experimental investigations. The nuclear science community is eagerly waiting for new or upgraded facilities to come online that can deliver high-intensity radioactive ion beams and expand the current reach of experimental investigations. The FRIB facility [75], for instance, has started operations in 2022 with reduced primary beam power (of 5 kW), and with the plan to continuously increase beam intensities until they reach their beam power ramp-up goal of 400 kW in 2028. The RIBF facility [93], currently the frontier facility for the study of exotic nuclei, has already planned its upgrade, delivering  $2\mu\text{A}$  of  $^{238}\text{U}$  primary beam by 2030. In Europe, the FAIR facility [117] is at the final stages of completion, and will be able to deliver high-energy exotic nuclei in a suite of different experimental setups. All these facilities, coupled to the development of new, more sensitive and sophisticated detection systems, set the stage for high discovery potential as well as detailed nuclear structure investigations, that will deliver unparalleled benchmarks to the ab initio frontier.

More importantly, what will decisively drive future developments and breakthroughs in our understanding of the atomic nucleus from first principles is the strong synergy between experiment and theory. We need to identify experimental benchmarks that can sensitively guide the theoretical developments, while the latter are trying to reproduce the nuclear landscape in a holistic approach, addressing as many observables as possible simultaneously. Such continuous feedback can only flourish within a strong nuclear science community, where experimentalists and theorists are working hand in hand to address overarching questions in physics and ultimately for mankind.

**Acknowledgements.** This work was supported by the Deutsche Forschungsgemeinschaft (DFG, German Research Foundation) Project-ID 279384907 - SFB 1245, the German Federal Ministry of Education and Research - BMBF project numbers 05P21RDFN2 and 05P21RDFNB, the Royal Society and the UK STFC awards ST/P003885/1, ST/V001035/1.

## References

- Weinberg S. 1990 Nuclear forces from chiral lagrangians. *Physics Letters B* **251**, 288–292. ([https://doi.org/10.1016/0370-2693\(90\)90938-3](https://doi.org/10.1016/0370-2693(90)90938-3))
- Machleidt R, Entem DR. 2011 Chiral effective field theory and nuclear forces. *Phys. Rept.* **503**, 1–75. ([10.1016/j.physrep.2011.02.001](https://doi.org/10.1016/j.physrep.2011.02.001))
- Epelbaum E, Hammer HW, Meissner UG. 2009 Modern Theory of Nuclear Forces. *Rev. Mod. Phys.* **81**, 1773–1825. ([10.1103/RevModPhys.81.1773](https://doi.org/10.1103/RevModPhys.81.1773))
- Epelbaum E, Meissner UG. 2012 Chiral dynamics of few- and many-nucleon systems. *Ann. Rev. Nucl. Part. Sci.* **62**, 159–185. ([10.1146/annurev-nucl-102010-130056](https://doi.org/10.1146/annurev-nucl-102010-130056))
- Lynn JE, Tews I, Carlson J, Gandolfi S, Gezerlis A, Schmidt KE, Schwenk A. 2016 Chiral Three-Nucleon Interactions in Light Nuclei, Neutron- $\alpha$  Scattering, and Neutron Matter. *Phys. Rev. Lett.* **116**, 062501. ([10.1103/PhysRevLett.116.062501](https://doi.org/10.1103/PhysRevLett.116.062501))
- Hebel K, Holt J, Menéndez J, Schwenk A. 2015 Nuclear Forces and Their Impact on Neutron-Rich Nuclei and Neutron-Rich Matter. *Annual Review of Nuclear and Particle Science* **65**, 457–484. ([10.1146/annurev-nucl-102313-025446](https://doi.org/10.1146/annurev-nucl-102313-025446))
- Kamada H et al.. 2001 Benchmark test calculation of a four nucleon bound state. *Phys. Rev. C* **64**, 044001. ([10.1103/PhysRevC.64.044001](https://doi.org/10.1103/PhysRevC.64.044001))
- Pudliner BS, Pandharipande VR, Carlson J, Wiringa RB. 1995 Quantum Monte Carlo calculations of  $A \leq 6$  nuclei. *Phys. Rev. Lett.* **74**, 4396–4399. ([10.1103/PhysRevLett.74.4396](https://doi.org/10.1103/PhysRevLett.74.4396))
- Carlson J, Gandolfi S, Pederiva F, Pieper SC, Schiavilla R, Schmidt KE, Wiringa RB. 2015 Quantum Monte Carlo methods for nuclear physics. *Rev. Mod. Phys.* **87**, 1067. ([10.1103/RevModPhys.87.1067](https://doi.org/10.1103/RevModPhys.87.1067))
- Navratil P, Vary JP, Barrett BR. 2000 Properties of C-12 in the ab initio nuclear shell model. *Phys. Rev. Lett.* **84**, 5728–5731. ([10.1103/PhysRevLett.84.5728](https://doi.org/10.1103/PhysRevLett.84.5728))
- Barrett BR, Navratil P, Vary JP. 2013 Ab initio no core shell model. *Prog. Part. Nucl. Phys.* **69**, 131–181. ([10.1016/j.pnpnp.2012.10.003](https://doi.org/10.1016/j.pnpnp.2012.10.003))
- Maris P, Vary JP, Calci A, Langhammer J, Binder S, Roth R. 2014  $^{12}\text{C}$  properties with evolved chiral three-nucleon interactions. *Phys. Rev. C* **90**, 014314. ([10.1103/PhysRevC.90.014314](https://doi.org/10.1103/PhysRevC.90.014314))
- Wiringa RB, Stoks VGJ, Schiavilla R. 1995 An Accurate nucleon-nucleon potential with charge independence breaking. *Phys. Rev. C* **51**, 38–51. ([10.1103/PhysRevC.51.38](https://doi.org/10.1103/PhysRevC.51.38))
- Machleidt R. 2001 The High precision, charge dependent Bonn nucleon-nucleon potential (CD-Bonn). *Phys. Rev. C* **63**, 024001. ([10.1103/PhysRevC.63.024001](https://doi.org/10.1103/PhysRevC.63.024001))
- Melendez JA, Wesolowski S, Furnstahl RJ. 2017 Bayesian truncation errors in chiral effective field theory: nucleon-nucleon observables. *Phys. Rev. C* **96**, 024003. ([10.1103/PhysRevC.96.024003](https://doi.org/10.1103/PhysRevC.96.024003))
- Melendez JA, Furnstahl RJ, Phillips DR, Pratola MT, Wesolowski S. 2019 Quantifying Correlated Truncation Errors in Effective Field Theory. *Phys. Rev. C* **100**, 044001. ([10.1103/PhysRevC.100.044001](https://doi.org/10.1103/PhysRevC.100.044001))
- Ekström A, Hagen G. 2019 Global sensitivity analysis of bulk properties of an atomic nucleus. *Phys. Rev. Lett.* **123**, 252501. ([10.1103/PhysRevLett.123.252501](https://doi.org/10.1103/PhysRevLett.123.252501))
- Suzuki K, Lee SY. 1980 Convergent Theory for Effective Interaction in Nuclei. *Prog. Theor. Phys.* **64**, 2091–2106. ([10.1143/PTP.64.2091](https://doi.org/10.1143/PTP.64.2091))

19. Bogner SK, Furnstahl RJ, Perry RJ. 2007 Similarity Renormalization Group for Nucleon-Nucleon Interactions. *Phys. Rev. C* **75**, 061001. ([10.1103/PhysRevC.75.061001](https://doi.org/10.1103/PhysRevC.75.061001))
20. Hergert H, Roth R. 2007 The Unitary correlation operator method from a similarity renormalization group perspective. *Phys. Rev. C* **75**, 051001. ([10.1103/PhysRevC.75.051001](https://doi.org/10.1103/PhysRevC.75.051001))
21. Bogner SK, Furnstahl RJ, Schwenk A. 2010 From low-momentum interactions to nuclear structure. *Prog. Part. Nucl. Phys.* **65**, 94–147. ([10.1016/j.ppnp.2010.03.001](https://doi.org/10.1016/j.ppnp.2010.03.001))
22. Roth R, Calci A, Langhammer J, Binder S. 2014 Evolved Chiral NN+3N Hamiltonians for Ab Initio Nuclear Structure Calculations. *Phys. Rev. C* **90**, 024325. ([10.1103/PhysRevC.90.024325](https://doi.org/10.1103/PhysRevC.90.024325))
23. Tichai A, Müller J, Vobig K, Roth R. 2019 Natural orbitals for ab initio no-core shell model calculations. *Phys. Rev. C* **99**, 034321. ([10.1103/PhysRevC.99.034321](https://doi.org/10.1103/PhysRevC.99.034321))
24. Roth R, Navrátil P. 2007 Ab initio study of Ca-40 with an importance truncated no-core shell model. *Phys. Rev. Lett.* **99**, 092501. ([10.1103/PhysRevLett.99.092501](https://doi.org/10.1103/PhysRevLett.99.092501))
25. Roth R. 2009 Importance Truncation for Large-Scale Configuration Interaction Approaches. *Phys. Rev. C* **79**, 064324. ([10.1103/PhysRevC.79.064324](https://doi.org/10.1103/PhysRevC.79.064324))
26. Maris P, Vary JP, Shirokov AM. 2009 Ab initio no-core full configuration calculations of light nuclei. *Phys. Rev. C* **79**, 014308. ([10.1103/PhysRevC.79.014308](https://doi.org/10.1103/PhysRevC.79.014308))
27. Coon SA, Avetian MI, Kruse MKG, van Kolck U, Maris P, Vary JP. 2012 Convergence properties of \it ab initio calculations of light nuclei in a harmonic oscillator basis. *Phys. Rev. C* **86**, 054002. ([10.1103/PhysRevC.86.054002](https://doi.org/10.1103/PhysRevC.86.054002))
28. Furnstahl RJ, Hagen G, Papenbrock T. 2012 Corrections to nuclear energies and radii in finite oscillator spaces. *Phys. Rev. C* **86**, 031301. ([10.1103/PhysRevC.86.031301](https://doi.org/10.1103/PhysRevC.86.031301))
29. More SN, Ekström A, Furnstahl RJ, Hagen G, Papenbrock T. 2013 Universal properties of infrared oscillator basis extrapolations. *Phys. Rev. C* **87**, 044326. ([10.1103/PhysRevC.87.044326](https://doi.org/10.1103/PhysRevC.87.044326))
30. Furnstahl RJ, Papenbrock T, More SN. 2014 Systematic expansion for infrared oscillator basis extrapolations. *Phys. Rev. C* **89**, 044301. ([10.1103/PhysRevC.89.044301](https://doi.org/10.1103/PhysRevC.89.044301))
31. Negoita GA et al.. 2019 Deep learning: Extrapolation tool for ab initio nuclear theory. *Phys. Rev. C* **99**, 054308. ([10.1103/PhysRevC.99.054308](https://doi.org/10.1103/PhysRevC.99.054308))
32. Jiang WG, Hagen G, Papenbrock T. 2019 Extrapolation of nuclear structure observables with artificial neural networks. *Phys. Rev. C* **100**, 054326. ([10.1103/PhysRevC.100.054326](https://doi.org/10.1103/PhysRevC.100.054326))
33. Knöll M, Wolfgruber T, Agel ML, Wenz C, Roth R. 2023 Machine learning for the prediction of converged energies from ab initio nuclear structure calculations. *Phys. Lett. B* **839**, 137781. ([10.1016/j.physletb.2023.137781](https://doi.org/10.1016/j.physletb.2023.137781))
34. Wolfgruber T, Knöll M, Roth R. 2023 Precise neural network predictions of energies and radii from the no-core shell model. .
35. Somà V. 2020 Self-consistent Green's function theory for atomic nuclei. *Front. in Phys.* **8**, 340. ([10.3389/fphy.2020.00340](https://doi.org/10.3389/fphy.2020.00340))
36. Gandolfi S, Lonardonì D, Lovato A, Piarulli M. 2020 Atomic nuclei from quantum Monte Carlo calculations with chiral EFT interactions. *Front. in Phys.* **8**, 117. ([10.3389/fphy.2020.00117](https://doi.org/10.3389/fphy.2020.00117))
37. Lähde TA, Meißner UG. 2019 *Nuclear Lattice Effective Field Theory: An introduction* vol. 957. Springer. ([10.1007/978-3-030-14189-9](https://doi.org/10.1007/978-3-030-14189-9))
38. Lynn JE, Tews I, Carlson J, Gandolfi S, Gezerlis A, Schmidt KE, Schwenk A. 2017 Quantum Monte Carlo calculations of light nuclei with local chiral two- and three-nucleon interactions. *Phys. Rev. C* **96**, 054007. ([10.1103/PhysRevC.96.054007](https://doi.org/10.1103/PhysRevC.96.054007))
39. Tichai A, Roth R, Duguet T. 2020 Many-body perturbation theories for finite nuclei. *Front. in Phys.* **8**, 164. ([10.3389/fphy.2020.00164](https://doi.org/10.3389/fphy.2020.00164))
40. Launey KD, Dytrych T, Sargsyan GH, Baker RB, Draayer JP. 2020 Emergent symplectic symmetry in atomic nuclei: Ab initio symmetry-adapted no-core shell model. *Eur. Phys. J. ST* **229**, 2429–2441. ([10.1140/epjst/e2020-000178-3](https://doi.org/10.1140/epjst/e2020-000178-3))
41. Yao JM, Engel J, Wang LJ, Jiao CF, Hergert H. 2018 Generator-coordinate reference states for spectra and  $0\nu\beta\beta$  decay in the in-medium similarity renormalization group. *Phys. Rev. C* **98**, 054311. ([10.1103/PhysRevC.98.054311](https://doi.org/10.1103/PhysRevC.98.054311))
42. Frosini M, Duguet T, Ebran JP, Bally B, Hergert H, Rodríguez TR, Roth R, Yao J, Somà V. 2022a Multi-reference many-body perturbation theory for nuclei: III. Ab initio calculations at second order in PGCM-PT. *Eur. Phys. J. A* **58**, 64. ([10.1140/epja/s10050-022-00694-x](https://doi.org/10.1140/epja/s10050-022-00694-x))
43. Frosini M, Duguet T, Ebran JP, Bally B, Mongelli T, Rodríguez TR, Roth R, Somà V. 2022b Multi-reference many-body perturbation theory for nuclei: II. Ab initio study of neon isotopes

- via PGCM and IM-NCSM calculations. *Eur. Phys. J. A* **58**, 63. ([10.1140/epja/s10050-022-00693-y](https://doi.org/10.1140/epja/s10050-022-00693-y))
44. Hagen G, Papenbrock T, Hjorth-Jensen M, Dean DJ. 2014 Coupled-cluster computations of atomic nuclei. *Rept. Prog. Phys.* **77**, 096302. ([10.1088/0034-4885/77/9/096302](https://doi.org/10.1088/0034-4885/77/9/096302))
  45. Tsukiyama K, Bogner SK, Schwenk A. 2011 In-Medium Similarity Renormalization Group for Nuclei. *Phys. Rev. Lett.* **106**, 222502. ([10.1103/PhysRevLett.106.222502](https://doi.org/10.1103/PhysRevLett.106.222502))
  46. Hergert H, Bogner SK, Morris TD, Schwenk A, Tsukiyama K. 2016 The In-Medium Similarity Renormalization Group: A Novel Ab Initio Method for Nuclei. *Phys. Rept.* **621**, 165–222. ([10.1016/j.physrep.2015.12.007](https://doi.org/10.1016/j.physrep.2015.12.007))
  47. Tsukiyama K, Bogner SK, Schwenk A. 2012 In-Medium Similarity Renormalization Group for Open-Shell Nuclei. *Phys. Rev. C* **85**, 061304. ([10.1103/PhysRevC.85.061304](https://doi.org/10.1103/PhysRevC.85.061304))
  48. Bogner SK, Hergert H, Holt JD, Schwenk A, Binder S, Calci A, Langhammer J, Roth R. 2014 Nonperturbative Shell-Model Interactions from the In-Medium Similarity Renormalization Group. *Phys. Rev. Lett.* **113**, 142501. ([10.1103/PhysRevLett.113.142501](https://doi.org/10.1103/PhysRevLett.113.142501))
  49. Jansen GR, Engel J, Hagen G, Navrátil P, Signoracci A. 2014 Ab Initio Coupled-Cluster Effective Interactions for the Shell Model: Application to Neutron-Rich Oxygen and Carbon Isotopes. *Phys. Rev. Lett.* **113**, 142502. ([10.1103/PhysRevLett.113.142502](https://doi.org/10.1103/PhysRevLett.113.142502))
  50. Hergert H. 2017 In-Medium Similarity Renormalization Group for Closed and Open-Shell Nuclei. *Phys. Scripta* **92**, 023002. ([10.1088/1402-4896/92/2/023002](https://doi.org/10.1088/1402-4896/92/2/023002))
  51. Sun ZH, Morris TD, Hagen G, Jansen GR, Papenbrock T. 2018 Shell-model coupled-cluster method for open-shell nuclei. *Phys. Rev. C* **98**, 054320. ([10.1103/PhysRevC.98.054320](https://doi.org/10.1103/PhysRevC.98.054320))
  52. Hergert H, Binder S, Calci A, Langhammer J, Roth R. 2013 Ab Initio Calculations of Even Oxygen Isotopes with Chiral Two-Plus-Three-Nucleon Interactions. *Phys. Rev. Lett.* **110**, 242501. ([10.1103/PhysRevLett.110.242501](https://doi.org/10.1103/PhysRevLett.110.242501))
  53. Hergert H, Bogner SK, Morris TD, Binder S, Calci A, Langhammer J, Roth R. 2014 Ab initio multireference in-medium similarity renormalization group calculations of even calcium and nickel isotopes. *Phys. Rev. C* **90**, 041302. ([10.1103/PhysRevC.90.041302](https://doi.org/10.1103/PhysRevC.90.041302))
  54. Gebrerufael E, Vobig K, Hergert H, Roth R. 2017 Ab Initio Description of Open-Shell Nuclei: Merging No-Core Shell Model and In-Medium Similarity Renormalization Group. *Phys. Rev. Lett.* **118**, 152503. ([10.1103/PhysRevLett.118.152503](https://doi.org/10.1103/PhysRevLett.118.152503))
  55. Ekström A, Hagen G, Morris TD, Papenbrock T, Schwartz PD. 2018  $\Delta$  isobars and nuclear saturation. *Phys. Rev. C* **97**, 024332. ([10.1103/PhysRevC.97.024332](https://doi.org/10.1103/PhysRevC.97.024332))
  56. Entem DR, Machleidt R, Nosyk Y. 2017 High-quality two-nucleon potentials up to fifth order of the chiral expansion. *Phys. Rev. C* **96**, 024004. ([10.1103/PhysRevC.96.024004](https://doi.org/10.1103/PhysRevC.96.024004))
  57. Reinert P, Krebs H, Epelbaum E. 2018 Semilocal momentum-space regularized chiral two-nucleon potentials up to fifth order. *Eur. Phys. J. A* **54**, 86. ([10.1140/epja/i2018-12516-4](https://doi.org/10.1140/epja/i2018-12516-4))
  58. Epelbaum E, Krebs H, Meißner UG. 2015 Precision nucleon-nucleon potential at fifth order in the chiral expansion. *Phys. Rev. Lett.* **115**, 122301. ([10.1103/PhysRevLett.115.122301](https://doi.org/10.1103/PhysRevLett.115.122301))
  59. Hüther T, Vobig K, Hebeler K, Machleidt R, Roth R. 2020 Family of Chiral Two- plus Three-Nucleon Interactions for Accurate Nuclear Structure Studies. *Phys. Lett. B* **808**, 135651. ([10.1016/j.physletb.2020.135651](https://doi.org/10.1016/j.physletb.2020.135651))
  60. Maris P et al.. 2021 Light nuclei with semilocal momentum-space regularized chiral interactions up to third order. *Phys. Rev. C* **103**, 054001. ([10.1103/PhysRevC.103.054001](https://doi.org/10.1103/PhysRevC.103.054001))
  61. Maris P et al.. 2022 Nuclear properties with semilocal momentum-space regularized chiral interactions beyond N2LO. *Phys. Rev. C* **106**, 064002. ([10.1103/PhysRevC.106.064002](https://doi.org/10.1103/PhysRevC.106.064002))
  62. Wesolowski S, Furnstahl RJ, Melendez JA, Phillips DR. 2019 Exploring Bayesian parameter estimation for chiral effective field theory using nucleon–nucleon phase shifts. *J. Phys. G* **46**, 045102. ([10.1088/1361-6471/aaf5fc](https://doi.org/10.1088/1361-6471/aaf5fc))
  63. Roth R. 2022 Ab Initio Approaches to Nuclear Structure. *Lect. Notes Phys.* **1005**, 87–139. ([10.1007/978-3-031-10751-1\\_3](https://doi.org/10.1007/978-3-031-10751-1_3))
  64. Friman-Gayer U et al.. 2021 Role of Chiral Two-Body Currents in  ${}^6\text{Li}$  Magnetic Properties in Light of a New Precision Measurement with the Relative Self-Absorption Technique. *Phys. Rev. Lett.* **126**, 102501. ([10.1103/PhysRevLett.126.102501](https://doi.org/10.1103/PhysRevLett.126.102501))
  65. Calci A, Roth R. 2016 Sensitivities and correlations of nuclear structure observables emerging from chiral interactions. *Phys. Rev. C* **94**, 014322. ([10.1103/PhysRevC.94.014322](https://doi.org/10.1103/PhysRevC.94.014322))
  66. Forssén C, Roth R, Navrátil P. 2013 Systematics of  $2^+$  states in C isotopes from the ab initio no-core shell model. *J. Phys. G* **40**, 055105. ([10.1088/0954-3899/40/5/055105](https://doi.org/10.1088/0954-3899/40/5/055105))
  67. Caprio MA, Fasano PJ, Maris P. 2022 Robust ab initio prediction of nuclear electric

- quadrupole observables by scaling to the charge radius. *Phys. Rev. C* **105**, L061302. ([10.1103/PhysRevC.105.L061302](https://doi.org/10.1103/PhysRevC.105.L061302))
68. Stroberg SR, Henderson J, Hackman G, Ruotsalainen P, Hagen G, Holt JD. 2022 Systematics of E2 strength in the sd shell with the valence-space in-medium similarity renormalization group. *Phys. Rev. C* **105**, 034333. ([10.1103/PhysRevC.105.034333](https://doi.org/10.1103/PhysRevC.105.034333))
69. NNDC - National Nuclear Data Centre. <https://www.nndc.bnl.gov/ensdf/>.
70. McCutchan EA, Lister CJ, Wiringa RB, Pieper SC, Seweryniak D, Greene JP, Carpenter MP, Chiara CJ, Janssens RVF, Khoo TL, Lauritsen T, Stefanescu I, Zhu S. 2009 Precise Electromagnetic Tests of Ab Initio Calculations of Light Nuclei: States in  $^{10}\text{Be}$ . *Phys. Rev. Lett.* **103**, 192501. ([10.1103/PhysRevLett.103.192501](https://doi.org/10.1103/PhysRevLett.103.192501))
71. McCutchan EA, Lister CJ, Pieper SC, Wiringa RB, Seweryniak D, Greene JP, Bertone PF, Carpenter MP, Chiara CJ, Gurdal G, Hoffman CR, Janssens RVF, Khoo TL, Lauritsen T, Zhu S. 2012 Lifetime of the  $2_1^+$  state in  $^{10}\text{C}$ . *Phys. Rev. C* **86**, 014312. ([10.1103/PhysRevC.86.014312](https://doi.org/10.1103/PhysRevC.86.014312))
72. Zanon I, Clément E, Goasduff A, Menéndez J, Miyagi T, Assié M, Ciemala M, Flavigny F, Lemasson A, Matta A, Ramos D, Rejmund M, Achouri L, Ackermann D, Barrientos D, Beaumel D, Benzoni G, Boston AJ, Boston HC, Bottoni S, Bracco A, Brugnara D, de France G, de Sereville N, Delaunay F, Desesquelles P, Didierjean F, Domingo-Prato C, Dudouet J, Eberth J, Fernández D, Fougères C, Gadea A, Galtarossa F, Girard-Alcindor V, Gonzales V, Gottardo A, Hammache F, Harkness-Brennan LJ, Hess H, Judson DS, Jungclaus A, Kaşkaş A, Kim YH, Kuşoğlu A, Labiche M, Leblond S, Lenain C, Lenzi SM, Leoni S, Li H, Ljungvall J, Lois-Fuentes J, Lopez-Martens A, Maj A, Menegazzo R, Mengoni D, Michelagnoli C, Million B, Napoli DR, Nyberg J, Pasqualato G, Podolyak Z, Pullia A, Quintana B, Recchia F, Regueira-Castro D, Reiter P, Rezyunkina K, Rojo JS, Salsac MD, Sanchis E, Şenyiğit M, Siciliano M, Sohler D, Stezowski O, Theisen C, Utepov A, Valiente-Dobón JJ, Verney D, Zielinska M. 2023 High-Precision Spectroscopy of  $^{20}\text{O}$  Benchmarking Ab Initio Calculations in Light Nuclei. *Phys. Rev. Lett.* **131**, 262501. ([10.1103/PhysRevLett.131.262501](https://doi.org/10.1103/PhysRevLett.131.262501))
73. Henderson SL, Ahn T, Caprio MA, Fasano PJ, Simon A, Tan W, O'Malley P, Allen J, Bardayan DW, Blankstein D, Frenzt B, Hall MR, Kolata JJ, McCoy AE, Moylan S, Reingold CS, Strauss SY, Torres-Isea RO. 2019 First measurement of the  $B(E2; 3/2^- \rightarrow 1/2^-)$  transition strength in  $^7\text{Be}$ : Testing *ab initio* predictions for  $A = 7$  nuclei. *Phys. Rev. C* **99**, 064320. ([10.1103/PhysRevC.99.064320](https://doi.org/10.1103/PhysRevC.99.064320))
74. Ciemala M, Ziliani S, Crespi FCL, Leoni S, Fornal B, Maj A, Bednarczyk P, Benzoni G, Bracco A, Boiano C, Bottoni S, Brambilla S, Bast M, Beckers M, Braunroth T, Camera F, Cieplicka-Oryńczak N, Clément E, Coelli S, Dorvaux O, Erturk S, de France G, Fransen C, Goldkuhle A, Grębosz J, Harakeh MN, Iskra LW, Jacquot B, Karpov A, Kicińska Habor M, Kim Y, Kmiecik M, Lemasson A, Lenzi SM, Lewitowicz M, Li H, Matea I, Mazurek K, Michelagnoli C, Matejska-Minda M, Million B, Müller-Gatermann C, Nanal V, Napiorkowski P, Napoli DR, Palit R, Rejmund M, Schmitt C, Stanoiu M, Stefan I, Vardaci E, Wasilewska B, Wieland O, Zieblinski M, Zielińska M, Ataç A, Barrientos D, Birkenbach B, Boston AJ, Cedervall B, Charles L, Collado J, Cullen DM, Désesquelles P, Domingo-Pardo C, Dudouet J, Eberth J, González V, Goupil J, Harkness-Brennan LJ, Hess H, Judson DS, Jungclaus A, Korten W, Labiche M, Lefevre A, Menegazzo R, Mengoni D, Nyberg J, Perez-Vidal RM, Podolyak Z, Pullia A, Recchia F, Reiter P, Saillant F, Salsac MD, Sanchis E, Stezowski O, Theisen C, Valiente-Dobón JJ, Holt JD, Menéndez J, Schwenk A, Simonis J. 2020 Testing *ab initio* nuclear structure in neutron-rich nuclei: Lifetime measurements of second  $2^+$  state in  $^{16}\text{C}$  and  $^{20}\text{O}$ . *Phys. Rev. C* **101**, 021303. ([10.1103/PhysRevC.101.021303](https://doi.org/10.1103/PhysRevC.101.021303))
75. FRIB - Facility for Rare Isotope Beams at Michigan State University. <https://frib.msu.edu>.
76. Vermeer W et al.. 1983 Electric quadrupole moment of the first excited state of  $^{12}\text{C}$ . *Phys. Lett. B* **122**, 23–26. ([https://doi.org/10.1016/0370-2693\(83\)91160-7](https://doi.org/10.1016/0370-2693(83)91160-7))
77. Raju MK et al.. 2018 Reorientation-effect measurement of the first  $2^+$  state in  $^{12}\text{C}$ : Confirmation of oblate deformation. *Phys. Lett. B* **777**, 250–254. (<https://doi.org/10.1016/j.physletb.2017.12.009>)
78. Saiz-Lomas J, Petri M, Lee I, Syndikus I, Heil S, Allmond J, Gaffney L, Pakarinen J, Badran H, Calverley T, Cox D, Forsberg U, Grahn T, Greenlees P, Hadynska-Klek K, Hilton J, Jenkinson M, Julin R, Konki J, Macchiavelli A, Mathy M, Ojala J, Papadakis P, Partanen J, Rahkila P, Ruotsalainen P, Sandzelius M, Saren J, Stolze S, Uusitalo J, Wadsworth R. 2023 The spectroscopic quadrupole moment of the  $2_1^+$  state of  $^{12}\text{C}$ : A benchmark of theoretical models.

- Physics Letters B **845**, 138114. (<https://doi.org/10.1016/j.physletb.2023.138114>)
79. D'Alessio A et al. 2020 Precision measurement of the  $E2$  transition strength to the  $2_1^+$  state of  $^{12}\text{C}$ . *Phys. Rev. C* **102**, 011302. ([10.1103/PhysRevC.102.011302](https://doi.org/10.1103/PhysRevC.102.011302))
  80. Epelbaum E, Krebs H, Lähde TA, Lee D, Meißner UG. 2012 Structure and Rotations of the Hoyle State. *Phys. Rev. Lett.* **109**, 252501. ([10.1103/PhysRevLett.109.252501](https://doi.org/10.1103/PhysRevLett.109.252501))
  81. Otsuka T, Abe T, Yoshida T, Tsunoda Y, Shimizu N, Itagaki N, Utsuno Y, Vary J, Maris P, Ueno H. 2022  $\alpha$ -Clustering in atomic nuclei from first principles with statistical learning and the Hoyle state character. *Nature Communications* **13**, 2234. ([10.1038/s41467-022-29582-0](https://doi.org/10.1038/s41467-022-29582-0))
  82. Sharon Y, Benczer-Koller N, Kumbartzki G, Zamick L, Casten R. 2018 Systematics of the ratio of electric quadrupole moments  $Q(2_1^+)$  to the square root of the reduced transition probabilities  $B(E2; 0_1^+ \rightarrow 2_1^+)$  in even-even nuclei. *Nuclear Physics A* **980**, 131–142. (<https://doi.org/10.1016/j.nuclphysa.2018.10.027>)
  83. Caprio MA, Fasano PJ. 2022 Ab initio estimation of  $E2$  strengths in  $^8\text{Li}$  and its neighbors by normalization to the measured quadrupole moment. *Phys. Rev. C* **106**, 034320. ([10.1103/PhysRevC.106.034320](https://doi.org/10.1103/PhysRevC.106.034320))
  84. Li H, Fang D, Ong HJ, Shirokov AM, Vary JP, Yin P, Zhao X. 2024 Quadrupole dynamics of carbon isotopes and  $^{10}\text{Be}$ . arXiv:2401.05776.
  85. Bijker R. 2019 Symmetries and order in cluster nuclei. *AIP Conference Proceedings* **2150**, 020002. ([10.1063/1.5124574](https://doi.org/10.1063/1.5124574))
  86. Marević P, Ebran JP, Khan E, Nikšić T, Vretenar D. 2019 Cluster structures in  $^{12}\text{C}$  from global energy density functionals. *Phys. Rev. C* **99**, 034317. ([10.1103/PhysRevC.99.034317](https://doi.org/10.1103/PhysRevC.99.034317))
  87. Yuan C, Suzuki T, Otsuka T, Xu F, Tsunoda N. 2012 Shell-model study of boron, carbon, nitrogen, and oxygen isotopes with a monopole-based universal interaction. *Phys. Rev. C* **85**, 064324. ([10.1103/PhysRevC.85.064324](https://doi.org/10.1103/PhysRevC.85.064324))
  88. Petri M, Paschalis S, Clark RM, Fallon P, Macchiavelli AO, Starosta K, Baugher T, Bazin D, Cartegni L, Crawford HL, Cromaz M, Datta Pramanik U, de Angelis G, Dewald A, Gade A, Grinyer GF, Gros S, Hackstein M, Jeppesen HB, Lee IY, McDaniel S, Miller D, Rajabali MM, Ratkiewicz A, Rother W, Voss P, Walsh KA, Weisshaar D, Wiedeking M, Brown BA, Forssén C, Navrátil P, Roth R. 2012 Structure of  $^{16}\text{C}$ : Testing shell model and ab initio approaches. *Phys. Rev. C* **86**, 044329. ([10.1103/PhysRevC.86.044329](https://doi.org/10.1103/PhysRevC.86.044329))
  89. Mathy M. 2020 *Electromagnetic Properties of Light Neutron-Rich Nuclei - Lifetime Measurements of  $^{16}\text{C}$  and  $^{23}\text{Ne}$* . PhD thesis Technischen Universität Darmstadt, Germany.
  90. Mathy M, Petri M, Roth R, Wagner L, Heil S et al.. 2024 Lifetimes of excited states in  $^{16}\text{C}$  as a benchmark for ab initio developments. submitted to *Eur. Phys. J A*.
  91. Petri M, Fallon P, Macchiavelli AO, Paschalis S, Starosta K, Baugher T, Bazin D, Cartegni L, Clark RM, Crawford HL, Cromaz M, Dewald A, Gade A, Grinyer GF, Gros S, Hackstein M, Jeppesen HB, Lee IY, McDaniel S, Miller D, Rajabali MM, Ratkiewicz A, Rother W, Voss P, Walsh KA, Weisshaar D, Wiedeking M, Brown BA. 2011 Lifetime Measurement of the  $2_1^+$  State in  $^{20}\text{C}$ . *Phys. Rev. Lett.* **107**, 102501. ([10.1103/PhysRevLett.107.102501](https://doi.org/10.1103/PhysRevLett.107.102501))
  92. Elekes Z, Dombrádi Z, Aiba T, Aoi N, Baba H, Bemmerer D, Brown BA, Furumoto T, Fülöp Z, Iwasa N, Kiss A, Kobayashi T, Kondo Y, Motobayashi T, Nakabayashi T, Nannichi T, Sakuragi Y, Sakurai H, Sohler D, Takashina M, Takeuchi S, Tanaka K, Togano Y, Yamada K, Yamaguchi M, Yoneda K. 2009 Persistent decoupling of valence neutrons toward the dripline: Study of  $^{20}\text{C}$  by  $\gamma$  spectroscopy. *Phys. Rev. C* **79**, 011302. ([10.1103/PhysRevC.79.011302](https://doi.org/10.1103/PhysRevC.79.011302))
  93. RIBF - Radioactive Isotope Beam Factory. <https://www.riken.jp/en/collab/resources/ribf/>.
  94. Gamma-Ray Energy Tracking Array. <https://greta.lbl.gov/>.
  95. HYPATIA: HYbrid Photon detector Array To Investigate Atomic nuclei. <https://www.nishina.riken.jp/collaboration/SUNFLOWER/devices/hypatia/index.php>.
  96. Otsuka T, Suzuki T, Holt JD, Schwenk A, Akaishi Y. 2010 Three-Body Forces and the Limit of Oxygen Isotopes. *Phys. Rev. Lett.* **105**, 032501. ([10.1103/PhysRevLett.105.032501](https://doi.org/10.1103/PhysRevLett.105.032501))
  97. Cipollone A, Barbieri C, Navrátil P. 2013 Isotopic chains around oxygen from evolved chiral two- and three-nucleon interactions. *Phys. Rev. Lett.* **111**, 062501. ([10.1103/PhysRevLett.111.062501](https://doi.org/10.1103/PhysRevLett.111.062501))
  98. Hebeler K, Holt JD, Menéndez J, Schwenk A. 2015 Nuclear forces and their impact on neutron-rich nuclei and neutron-rich matter. *Ann. Rev. Nucl. Part. Sci.* **65**, 457.
  99. Stroberg SR, Holt JD, Schwenk A, Simonis J. 2021 Ab Initio Limits of Atomic Nuclei. *Phys. Rev. Lett.* **126**, 022501. ([10.1103/PhysRevLett.126.022501](https://doi.org/10.1103/PhysRevLett.126.022501))

100. Holt JD, Menéndez J, Schwenk A. 2013 Chiral three-nucleon forces and bound excited states in neutron-rich oxygen isotopes. *Eur. Phys. J. A* **49**, 39. ([10.1140/epja/i2013-13039-2](https://doi.org/10.1140/epja/i2013-13039-2))
101. Caesar C et al.. 2013 Beyond the Neutron Drip-Line: The Unbound Oxygen Isotopes  $^{25}\text{O}$  and  $^{26}\text{O}$ . *Phys. Rev. C* **88**, 034313. ([10.1103/PhysRevC.88.034313](https://doi.org/10.1103/PhysRevC.88.034313))
102. Heil S, Petri M, Vobig K, Bazin D, Belarge J, Bender P, Brown B, Elder R, Elman B, Gade A, Haylett T, Holt J, Hüther T, Hufnagel A, Iwasaki H, Kobayashi N, Loelius C, Longfellow B, Lunderberg E, Mathy M, Menéndez J, Paschalis S, Roth R, Schwenk A, Simonis J, Syndikus I, Weisshaar D, Whitmore K. 2020 Electromagnetic properties of  $^{21}\text{O}$  for benchmarking nuclear Hamiltonians. *Phys. Lett. B* **809**, 135678. ([10.1016/j.physletb.2020.135678](https://doi.org/10.1016/j.physletb.2020.135678))
103. Petri M. 2024 Electromagnetic transition rates in  $^{21}\text{O}$ . ATLAS, Argonne National Laboratory, Experiment #2044.
104. Entem DR, Machleidt R. 2003 Accurate charge-dependent nucleon-nucleon potential at fourth order of chiral perturbation theory. *Phys. Rev. C* **68**, 041001. ([10.1103/PhysRevC.68.041001](https://doi.org/10.1103/PhysRevC.68.041001))
105. Roth R, Binder S, Vobig K, Calci A, Langhammer J, Navrátil P. 2012 Medium-Mass Nuclei with Normal-Ordered Chiral  $NN+3N$  Interactions. *Phys. Rev. Lett.* **109**, 052501. ([10.1103/PhysRevLett.109.052501](https://doi.org/10.1103/PhysRevLett.109.052501))
106. Ekström A, Jansen GR, Wendt KA, Hagen G, Papenbrock T, Carlsson BD, Forsén C, Hjorth-Jensen M, Navrátil P, Nazarewicz W. 2015 Accurate nuclear radii and binding energies from a chiral interaction. *Phys. Rev. C* **91**, 051301. ([10.1103/PhysRevC.91.051301](https://doi.org/10.1103/PhysRevC.91.051301))
107. Thirolf PG, Pritychenko BV, Brown BA, Cottle PD, Chromik M, Glasmacher T, Hackman G, Ibbotson RW, Kemper KW, Otsuka T et al.. 2000 Spectroscopy of the  $2_1^+$  state in  $^{22}\text{O}$  and shell structure near the neutron drip line. *Phys. Lett. B* **485**, 16 – 22.
108. Paschalis S, Lee I, Macchiavelli A, Campbell C, Cromaz M, Gros S, Pavan J, Qian J, Clark R, Crawford H, Doering D, Fallon P, Lionberger C, Loew T, Petri M, Stezelberger T, Zimmermann S, Radford D, Lagergren K, Weisshaar D, Winkler R, Glasmacher T, Anderson J, Beausang C. 2013 The performance of the Gamma-Ray Energy Tracking In-beam Nuclear Array GRETINA. *Nuclear Instruments and Methods in Physics Research Section A: Accelerators, Spectrometers, Detectors and Associated Equipment* **709**, 44–55. (<https://doi.org/10.1016/j.nima.2013.01.009>)
109. Petri M. 2021 Electromagnetic transition rates in  $^{22}\text{O}$  and  $^{23}\text{F}$ . ATLAS, Argonne National Laboratory, Experiment #1732.
110. Tetley L. 2022 The Structure of the Neutron-Rich  $^{22}\text{O}$  and  $^{23}\text{F}$  Nuclides. PhD thesis University of York, UK.
111. Tetley L, Maugeri EA, Petri M, Schumann D. 2021 Preparation of a thin  $^{10}\text{Be}$  target for nuclear structure experiments. *Annual Report 2021, Laboratory of Radiochemistry, Paul Scherrer Institut.*
112. Tetley L, Maugeri EA, Petri M, Schumann D, Lagoyannis A. 2019 Preparation of a  $^{10}\text{Be}$  target on a carbon backing for nuclear structure measurements. *Annual Report 2019, Laboratory of Radiochemistry, Paul Scherrer Institut.*
113. Wimmer K LISA: Lifetime measurements with Solid Active targets. ERC Consolidator Grant 101001561-LISA.
114. Williams J, Ball GC, Chester A, Domingo T, Garnsworthy AB, Hackman G, Henderson J, Henderson R, Krücken R, Kumar A, Launey KD, Measures J, Paetkau O, Park J, Sargsyan GH, Smallcombe J, Srivastava PC, Starosta K, Svensson CE, Whitmore K, Williams M. 2019 Structure of  $^{28}\text{Mg}$  and influence of the neutron  $pf$  shell. *Phys. Rev. C* **100**, 014322. ([10.1103/PhysRevC.100.014322](https://doi.org/10.1103/PhysRevC.100.014322))
115. Henderson J, Hackman G, Ruotsalainen P, Holt JD, Stroberg SR, Andreoiu C, Ball GC, Bernier N, Bowry M, Caballero-Folch R, Cruz S, Diaz Varela A, Evitts LJ, Frederick R, Garnsworthy AB, Holl M, Lassen J, Measures J, Olaizola B, O'Sullivan E, Paetkau O, Park J, Smallcombe J, Svensson CE, Whitmore K, Wu CY. 2022 Coulomb excitation of the  $|T_z| = \frac{1}{2}$ ,  $A = 23$  mirror pair. *Phys. Rev. C* **105**, 034332. ([10.1103/PhysRevC.105.034332](https://doi.org/10.1103/PhysRevC.105.034332))
116. Garnsworthy AB, Bowry M, Olaizola B, Holt JD, Stroberg SR, Cruz S, Georges S, Hackman G, MacLean AD, Measures J, Patel HP, Pearson CJ, Svensson CE. 2017 Spectroscopy of  $^{50}\text{Sc}$  and ab initio calculations of  $B(M3)$  strengths. *Phys. Rev. C* **96**, 044329. ([10.1103/PhysRevC.96.044329](https://doi.org/10.1103/PhysRevC.96.044329))
117. FAIR - Facility for Antiproton and Ion Research. <https://fair-center.eu>.